Renormalized perturbation approach to instanton-noninstanton transition in nearly integrable tunneling processes

Yasutaka Hanada
Department of Electrical Engineering, Faculty of Science and Engineering, Kyushu Sangyo University, 3-1-2 Matsukadai, Higashi-ku, Fukuoka 813-8503, Japan

Akira Shudo
Department of Physics, Tokyo Metropolitan University, Minami-Osawa, Hachioji, Tokyo 192-0397, Japan

Teruaki Okushima
Science and Technology Section, General Education Division, College of Engineering, Chubu University, Matsumoto-cho, Kasugai, Aichi 487-8501, Japan

Kensuke S. Ikeda
College of Science and Engineering, Ritsumeikan University Noji-higashi 1-1-1, Kusatsu 525, Japan

(Received 10 June 2018; published 2 May 2019)

A renormalized perturbation method is developed for quantum maps of periodically kicked rotor models to study the tunneling effect in the nearly integrable regime. Integrable Hamiltonians closely approximating the nonintegrable quantum map are systematically generated by the Baker-Hausdorff-Campbell (BHC) expansion for symmetrized quantum maps. The procedure results in an effective integrable renormalization, and the unrenormalized residual part is treated as the perturbation. If a sufficiently high-order BHC expansion is used as the base of perturbation theory, the lowest order perturbation well reproduces tunneling characteristics of the quasibound eigenstates, including the transition from the instanton tunneling to a noninstanton one. This approach enables a comprehensive understanding of the *purely quantum mechanisms* of tunneling in the nearly integrable regime. In particular, the staircase structure of tunneling probability dependence on quantum number can be clearly explained as the successive transition among multiquanta excitation processes. The transition matrix elements of the residual interaction have resonantly enhanced invariant components that are not removed by the renormalization. Eigenmodes coupled via these invariant components form noninstanton (NI) tunneling channels of two types contributing to the two regions of each step of the staircase structure: one type of channel is inside the separatrix, and the other goes across the separatrix. The amplitude of NI tunneling across the separatrix is insensitive to the Planck constant but shows an essentially singular dependence upon the nonintegrablity parameter. Its relation to the Melnikov integral, which characterizes the scale of classical chaos emerging close to the saddle on the potential top, is discussed.

DOI: 10.1103/PhysRevE.99.052201

I. INTRODUCTION

Poincaré proved that an arbitrary small perturbation applied to integrable systems almost always makes it nonintegrable, and he stressed that the study of perturbed integrable systems is the "fundamental problem of dynamics" [1], because topologically the phase space of a perturbed integrable system becomes pathological. Later, Kolmogorov, Arnold, and Moser (KAM) proved that in nearly integrable systems the nonintegrability is noncatastrophic in the sense of measure, as it should be [2]. Indeed, in nearly integrable systems most of the tori which fill the phase space in the integrable limit still survive as the KAM tori and the measure of chaotic region is exponentially small as $\sim e^{-\mathrm{const}/\epsilon^{1/2}}$, where ϵ is the strength of perturbation [3,4].

Quantum mechanically, the tori filling the phase space in the integrable limit are quantized according to the semiclassical rule of action quantization and form the support of eigenfunctions. Each torus is analytic in the real plane, and it can be analytically continued into the complex domain and forms the set supporting the tunneling part of wave function. The section of the complexified torus with the real plane representing the observable is called the *instanton* [5]. In the nearly integrable regime, almost all of the KAM tori still survive, and they are quantized according to the Einstein-Brillouin-Keller (EBK) quantization rule [6], which is a generalized version of the action quantization rule. Thus, the effect of nonintegrability on the quantized state is negligibly small in the real phase space. However, the significant change of dynamical structure caused by nonintegrability first manifests itself in the complexified phase space [7,8].

The effect of nonintegrability first emerges on the complexified part of the torus as the *natural boundary* [8], a dense set of singularities, which destroys the analyticity of the KAM torus in the complex domain. The instanton is thus in general interrupted by the natural boundary [9].

The tunneling component of the EBK quantized wave function may drastically be distorted beyond the natural boundary. The tunneling theory based on classically integrable complexified tori [10] may not be applicable in the nearly integrable regime [11]. Indeed, a numerical study revealed that the tunneling component starts to drastically increase beyond the natural boundary [12]. This suggests that nonintegrability manifests itself very sensitively as tunneling phenomena.

Over the last two decades the interest in nonintegrability and tunneling has been gradually growing [13,14]. With Ref. [15], the complex domain semiclassical theory [16] was first applied to the study of chaotic tunneling in quantum map systems, and it has been revealed that the complexified stable-unstable manifolds (CSUMs) of unstable saddles form the skeleton of tunneling orbits [17], which physically means that chaos attracts the tunneling orbit toward the real phase space [18]. This is a complex-semiclassical interpretation for the remarkable enhancement of tunneling probability by chaos [19], which is often called chaos-assisted tunneling [20,21]. Mathematically, the CSUM mechanism means that the Julia set plays a central role in tunneling problem [17].

On the other hand, the complex semiclassical method was developed for a continuous-time nonintegrable scattering system in Ref. [22], and it was confirmed that the CSUM mechanism plays the central role [23,24] and it was shown that a crossover from the instanton to the CSUM mechanism occurs. However, in this model chaos does not exist in the real phase space. In most general cases of a nearly integrable regime chaos exists in the real phase space, although its measure is exponentially small. It has still not been clarified how the transition from instanton to some other tunneling process takes place in a nearly integrable regime.

Since nonlinear resonances emerge when a perturbation is added to integrable systems, it would be natural to examine their effect on quantum tunneling. The idea of the so-called resonance-assisted tunneling (RAT) is that utilizing the coupling via nonlinear resonances one may obtain more efficient tunneling channels, which bypass the original instanton. The actual calculation scheme based on such an idea was first proposed in Ref. [25] and applied to a couple of systems later [26,27]. After some improvements, the validity of the scheme was further tested for more controlled situations [28–30]. In parallel, the RAT calculation was performed for a one-dimensional normal form Hamiltonian [31], which is supposed to ideally model RAT. In the same spirit integrable approximation to nonintegrable situations has been developed [32].

The transition from the instanton to noninstanton tunneling, which we hereafter refer to as the instanton-noninstanton (I-NI) transition, is an important issue, which has not been elucidated yet. The complex semiclassical theory for the I-NI transition has been presented only for scattering systems in which chaos does not appear in the real phase space [22–24].

In a previous paper we have closely studied $1/\hbar$-dependence of tunneling splitting in a nearly integrable regime and found that the splitting curve should be viewed as the staircase-shaped skeleton accompanied by spikes. In particular we have revealed that the plateau, whose origin has often been a problem [26–28], is formed as a result of tunneling coupling across the separatrix [33,34], and so it would be beyond the perspective of the RAT theory.

In the present paper, we investigate the quantum mechanism dominating the characteristic behavior of a nonintegrable tunneling process including the I-NI transition in the nearly integrable regime. Instead of observing $1/\hbar$-dependence of tunneling probability, we investigate the quantum number dependence of the tunneling probability as the main tunneling characteristic.

The method used here is a renormalized perturbation method proposed in Ref. [34]: it uses an integrable Hamiltonian very closely approximating the quantum map as the renormalized base, which is constructed systematically by the Baker-Hausdorff-Campbell expansion. Taking the unrenormalized residual interaction as the perturbation source, we develop a perturbation theory which is very effective to elucidate the interplay between two parts of the Hamiltonian: the part renormalized as an integrable Hamiltonian and the unrenormalizable residual interaction. This interplay controls the tunneling characteristics and provides a simple interpretation to the noninstanton tunneling. In this sense this approach provides a fully quantum mechanical understanding for tunneling in nearly integrable regime.

First, we show in Figs. 1(a) and 1(b) typical examples of tunneling probabilities of quasibound eigenstates through a one-dimensional potential barrier in the nearly integrable regime. They are obtained for (a) the Hénon map and (b) the standard map by the exact numerical diagonalization and are plotted as a function of quantum number n [34]. As discussed in detail later, for small nonintegrability parameter, the quantum map is very well approximated by the one-dimensional barrier tunneling Hamiltonian, which is, of course, integrable, and the eigenstates of the integrable Hamiltonian are very good approximations to those of the quantum map. We can expect that the tunneling components of the integrable system are well approximated by the instanton model depicted by the broken lines of Figs. 1(a) and 1(b). However, as the quantum number decreases from the top, the tunneling probability suddenly increases from the instanton probability for a quantum number below a characteristic number denoted by n_c, and next form a remarkable "plateau", whose height is insensitive to the Planck constant. We also note that the corresponding classical Poincaré maps in Figs. 1(a) and 1(b) exhibit typical flow patterns of the integrable system and do not show any visible signatures of nonlinear resonances and chaos. The above facts suggest that, as has been often stressed, the tunneling effect is very sensitive to nonintegrability.

The outline of the present paper is as follows. In the next section nonintegrable quantum maps used in Fig. 1 and throughout the present paper are introduced in a symmetrized form. The Baker-Hausdorff-Campbell (BHC) expansion for the symmetrized quantum maps is applied to constructing a series of integrable Hamiltonians, which approximates the quantum map with systematically increasing precision. It is shown that the lowest-order perturbation theory using the residual part of the quantum map, which cannot be renormalized as the integrable Hamiltonian, agrees quite well with the results obtained by the exact numerical diagonalization demonstrated in Fig. 1, if a fully higher-order BHC integrable Hamiltonian is taken as the basis.

In Sec. III the physical origin of the tunneling characteristics such as the I-NI transition and the staircase structure are

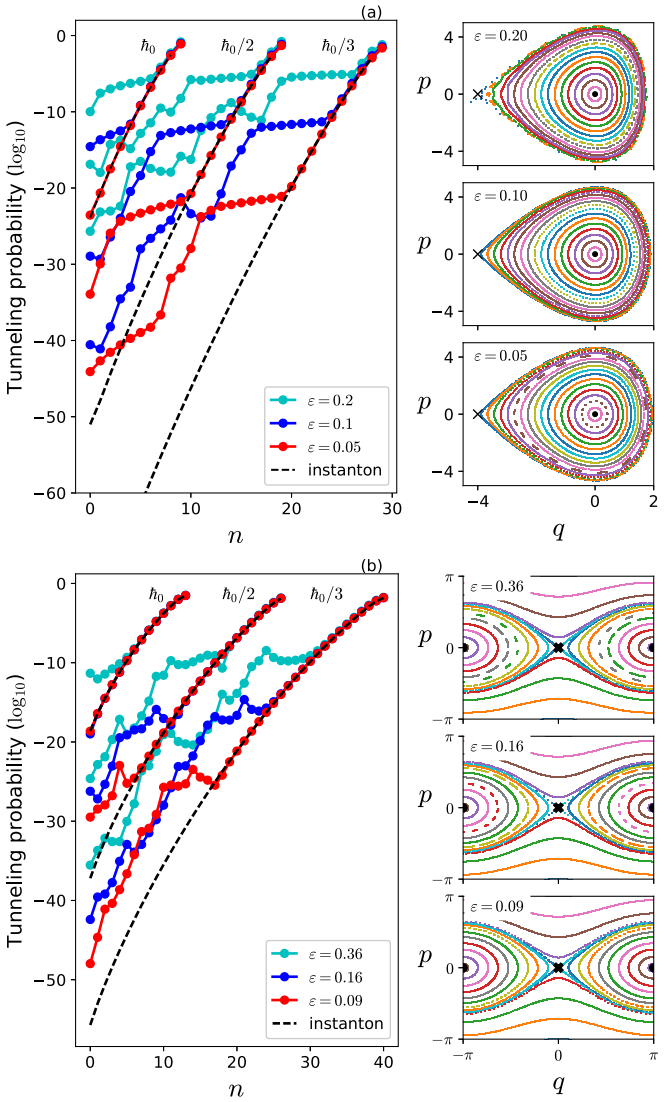

FIG. 1. Typical examples of tunneling probability of eigenstates vs quantum number measured at the tunneling tail of a wave function. (a) The Hénon map and (b) the standard map for three values of the Planck constant $\hbar = \hbar_0$, $\hbar_0/2$, $\hbar_0/3$ and three values of nonintegrability parameter ϵ. The classical Poincaré cross sections corresponding to three values of ϵ are also depicted on the right-hand side, where • and × indicate, respectively, the elliptic point O and the saddle point S. The definition of $\hbar_0$ is given in Fig. 2.

explained with a crucial property possessed by the transition matrix elements (TMEs) of the residual evolution operator with respect to the eigenstates of the integrable Hamiltonian: the transition matrix has the resonantly enhanced invariant elements unrenormalizable as the effective integrable Hamiltonian, which select specific modes as the noninstanton (NI) tunneling channels. Moreover, the amplitude of invariant elements, which characterizes the NI tunneling amplitude, is insensitive to the Planck constant and exhibits essentially singular behavior with respect to the parameter controlling nonintegrability. Such behavior is very similar to the Melnikov integral characterizing the measure of classical chaos in nearly integrable regime. A possible origin of such a behavior is discussed based on the correspondence principle. With these arguments we finally present a simple picture explaining the tunneling characteristics in the nearly integrable regime, and discuss how the above mechanism is reflected in the phase space structure of eigenfunctions.

Section IV is devoted to the summary and conclusion of the present paper.

II. QUANTUM MAP AND AN INTEGRABILITY-BASED PERTURBATION THEORY

We consider two typical types of barrier tunneling in nonintegrable systems. In one case the system is open to infinity and the probability of eigenstates leaks through the barrier, which results in the finite lifetime of the eigenstate. In another case the system is closed and the tunneling through the barrier of the symmetric potential results in the spectrum doublet. We take the symmetric form of the quantum maps

$$\hat{U} = e^{-i\hat{P}^2/4\hbar} e^{-i\epsilon V(\hat{Q})/\hbar} e^{-i\hat{P}^2/4\hbar} \tag{1}$$

of the kicked rotor model described by the periodically δ-kicked Hamiltonian

$$\hat{H} = \hat{P}^2/2 + \epsilon V(\hat{Q}) \sum_{n=-\infty}^{+\infty} \delta(t - n - 1/2). \tag{2}$$

This map describes the unit time evolution by Eq. (2) and consists of two free-evolution operators $e^{-i\hat{P}^2/4\hbar}$ for the time interval $1/2$ between which a kick operation $e^{-i\epsilon V(\hat{Q})/\hbar}$ is inserted. The symmetrization makes it easier to construct the higher-order integrable approximation, as will be discussed later. On the other hand, in the case of the standard map we use the alternative form

$$\hat{U} = e^{-i\epsilon V(\hat{Q})/2\hbar} e^{-i\hat{P}^2/2\hbar} e^{-i\epsilon V(\hat{Q})/2\hbar}, \tag{3}$$

in which the order of the kick and the free evolution are exchanged, because of some technical reasons. The potential functions for the Hénon map and the standard map are, respectively, given as

$$\text{Hénon map} \quad V(\hat{Q}) = 2\hat{Q}^2 + \hat{Q}^3/3, \tag{4}$$

$$\text{standard map} \quad V(\hat{Q}) = \cos\hat{Q}, \tag{5}$$

respectively.

The time evolution of the classical dynamics corresponding to Eqs. (1) and (3) is, respectively, expressed as the the mapping rule

$$\begin{pmatrix} Q' \\ P' \end{pmatrix} = \begin{pmatrix} Q + P - \epsilon V'(Q + P/2)/2 \\ P - \epsilon V'(Q + P/2) \end{pmatrix} \tag{6}$$

and

$$\begin{pmatrix} Q' \\ P' \end{pmatrix} = \begin{pmatrix} Q + P - V'(Q)/2 \\ P - \epsilon V'(Q)/2 - \epsilon V'[Q + P - \epsilon V'(Q)/2)] \end{pmatrix}, \tag{7}$$

both of which are conjugate to the so-called Hénon map and the standard map, respectively. Note that the Hénon map is an open system having a superattractor at $(Q, P) = (-\infty, -\infty)$ to which the tunneling wave packet is transported.

For the treatment of the open system, such as the Hénon map, we need to introduce an imaginary absorbing potential to $V(Q)$ at the ends of the computational space, but the location

of the absorber is very carefully chosen because it often damages the original nature of tunneling drastically.

Introducing the imaginary potential breaks the unitarity of $\hat{U}$, and the Hermite conjugacy of wave function is lost. However, if we take the q-representation for the evolution operator, the unitary evolution operator, which includes the absorption potential in the potential part, can be made symmetric, and the right eigenfunction is identified with the left eigenfunction. Thus, the inner product of eigenfunctions can simply be expressed as

$$\langle u|v\rangle = \int_{-\infty}^{\infty} u(Q)v(Q)\,dQ. \tag{8}$$

On the other hand, the standard map is a closed conservative system. We define the potential function $\epsilon V(Q) = \epsilon\cos Q$ in the extended range $-2\pi \leqslant Q < 2\pi$ and impose the periodic boundary condition identifying $Q = -2\pi$ with $Q = 2\pi$. The potential $\epsilon V(Q)$ has two equivalent valleys bottomed at $Q = -\pi$ and $Q = \pi$ symmetric with respect to the barriers peaked at $Q = 0$ and $Q = \pm 2\pi$. For the eigenfunction with the energy less than the potential barrier of height ϵ, the parity symmetry $Q \to -Q$ induces the degeneracy if the barrier isolates the two valleys. Tunneling, however, resolves the degeneracy and makes a doublet whose energy difference is called tunneling splitting.

To describe the transition process from the instanton mechanism working in the integrable limit, it is natural to develop a perturbation theory based on the integrable Hamiltonian. To make clear the integrable limit of quantum maps, we introduce the new effective Planck constant,

$$\hbar = \hbar/\sqrt{\epsilon}, \tag{9}$$

and introduce the new momentum and coordinate operator:

$$\hat{p} = -i\hbar d/d\hat{q}, \quad \hat{q} = \hat{Q}. \tag{10}$$

Then $\hat{U}$ becomes a convenient form for our approach:

$$\hat{U} = e^{-i\frac{\sqrt{\epsilon}}{\hbar}\frac{\hat{p}^2}{4}} e^{-i\frac{\sqrt{\epsilon}}{\hbar}V(\hat{q})} e^{-i\frac{\sqrt{\epsilon}}{\hbar}\frac{\hat{p}^2}{4}}. \tag{11}$$

Regarding $\hbar$ as the effective Planck constant, the fundamental period of the kick is interpreted as $\sqrt{\epsilon}$, and the fundamental energy quanta related to the period are given by

$$\Omega\hbar = 2\pi\hbar/\epsilon, \tag{12}$$

which plays an important role later. Here $\frac{\sqrt{\epsilon}}{\hbar} = \frac{\epsilon}{\hbar}$, and in the small limit of $\frac{\sqrt{\epsilon}}{\hbar} \ll 1$ it is well known that the unitary operator with the Hamiltonian $H_{\rm eff}^{(1)}$

$$\hat{U}^{(1)} = e^{-i\frac{\sqrt{\epsilon}}{\hbar}H_{\rm eff}^{(1)}}, \qquad H_{\rm eff}^{(1)} = \hat{p}^2/2 + V(\hat{q}), \tag{13}$$

approximates $\hat{U}$ and the residual part $\Delta\hat{U}^{(1)} := \hat{U} - \hat{U}^{(1)}$ is estimated as $O(\frac{\sqrt{\epsilon}}{\hbar}^3)$. However, the magnitude of the residual operator $\Delta\hat{U}^{(1)}$ is larger than the exponentially small tunneling tail of the wave function unless ϵ is much less than the tunneling strength. This implies the perturbation approach taking Eq. (13) as the lowest order Hamiltonian makes no sense.

By applying the Baker-Hausdorff-Campbell (BHC) expansion to the product of incommutable operators forming the quantum maps, one can construct a series of integrable Hamiltonians approximating the quantum map with systematically improved accuracy. Let us introduce an approximate Hamiltonian called the BHC Hamiltonian, which is a series of expansion in powers of the smallness parameter $s = -i\frac{\sqrt{\epsilon}}{\hbar}$:

$$H_{\rm eff}^{(M)} = \sum_{\ell=1,3,\ldots,M} s^{\ell-1} H_\ell. \tag{14}$$

The coefficient H_ℓ is decided in such a way that the expansion of the exponentiated operator $\hat{U}^{(M)} = e^{sH_{\rm eff}^{(M)}}$ in powers of s agrees with that of $\hat{U}$. This expansion is no more than the BHC expansion of the product of operators. The reason why the expansion (14) contains only the terms with even power of s is that because of the symmetrized form of $\hat{U}$ the inverse operator $\hat{U}^{-1}$ can be given simply by setting $s \to -s$, that is, $\hat{U}(s)\hat{U}(-s) = 1$. With this expansion, we can recursively show that H_ℓ begins with the $\ell - 1$-th commutation relation and its lowest-order term starts with a term of $O(\hbar^{\ell-1})$, and H_ℓ can be expressed by a finite power series of $\hbar$:

$$H_\ell = \hbar^{\ell-1}\mathcal{H}_\ell, \quad \mathcal{H}_\ell = \sum_{k=0}^{k_\ell} \hbar^k h_\ell^{(k)}. \tag{15}$$

In particular if the potential is a polynomial such as in the case of the Hénon map, the kth-order coefficient Hamiltonian is a polynomial of $\hat{q}$, $\hat{p}$. In the case of the standard map, the kth-order coefficient is a finite-degree polynomial of $\cos q$, $\sin q$. In the case of the Hénon map, for example,

$$h_\ell^{(k)} = \sum_{\substack{0 \leqslant i \leqslant i_{\max} \\ 0 \leqslant j \leqslant j_{\max}}} C(\ell, k, i, j)\hat{q}^i\hat{p}^j, \tag{16}$$

where $i_{\max}$ and $j_{\max}$ depend upon (ℓ, k). The algebraic manipulation program of Mathematica is used for computing the polynomials. Finally, the unitary evolution operator based on the Mth-order BHC Hamiltonian is

$$\hat{U}^{(M)} = \exp\left\{-i\frac{\sqrt{\epsilon}}{\hbar}H_{\rm eff}^{(M)}\right\}, \tag{17}$$

$$\text{where } H_{\rm eff}^{(M)} = \sum_{\ell=1,3,5,\ldots,M} (-\epsilon)^{\frac{\ell-1}{2}}\mathcal{H}_\ell, \tag{18}$$

is the Mth-order BHC Hamiltonian. Note that the above Hamiltonian with $k = 0$ in the expansion (15) gives the classical BHC Hamiltonian. As the approximation order M increases, $\hat{U}^{(M)}$ approximates $\hat{U}$ more closely, but the absolute convergence for $M \to \infty$ is not guaranteed if $|s|$ is not very small. The convergence is generally thought to be asymptotic and so there exists an optimal M [35].

Taking the BHC Hamiltonian of a large M as the lowest order Hamiltonian, we can develop a perturbation theory regarding the extremely small residual operator

$$\delta\hat{U}^{(M)} = \hat{U} - \hat{U}^{(M)} = O\left[\left(i\frac{\sqrt{\epsilon}}{\hbar}\right)(-\epsilon)^{(M+1)/2}\right] \tag{19}$$

as the perturbation. We call $\delta\hat{U}^{(M)}$ the Mth-order residual operator.

Let $|u_n^M\rangle$ and $E_n^{(M)}$ be the nth eigenstate and eigenenergy of $H_{\rm eff}^{(M)}$, where the quantum number is assigned in the ascending

order, taking $n = 0$ as the ground state. Then the lowest-order perturbed eigenstate is simply given by

$$\left|\psi_n^{(M)}\right\rangle = \left|u_n^{(M)}\right\rangle + \sum_j R_{nj}^{(M)} \left\langle u_j^{(M)}\right| \delta\hat{U}^{(M)} \left|u_n^{(M)}\right\rangle \left|u_j^{(M)}\right\rangle, \quad (20)$$

where $R_{nj}^{(M)}$ is the resonance factor defined by

$$R_{nj}^{(M)} = 1/(e^{-i\frac{\sqrt{\epsilon}}{k}E_n^{(M)}} - e^{-i\frac{\sqrt{\epsilon}}{k}E_j^{(M)}}). \quad (21)$$

On the other hand, the perturbed eigenenergy is given by

$$e^{-i\Omega_n} = e^{-i\frac{\sqrt{\epsilon}}{k}E_j^{(M)}} + \left\langle u_n^{(M)}\right| \delta\hat{U}^{(M)} \left|u_n^{(M)}\right\rangle + \sum_{j\neq n} \left\langle u_n^{(M)}\right| \delta\hat{U}^{(M)} \left|u_j^{(M)}\right\rangle \left\langle u_j^{(M)}\right| \delta\hat{U}^{(M)} \left|u_n^{(M)}\right\rangle R_{nj}^{(M)}. \quad (22)$$

We discuss the classical phase space of the integrable Hamiltonian and its semiclassical quantization together with the semiclassical tunneling process in it. If ϵ is small, the lowest-order Hamiltonian (13) classically provides a good approximation to the dynamics of the classical maps (6) and (7), and the higher-order Hamiltonian $H_{\rm eff}^{(M)}$ further improves the approximation, but the topology of classical flow is invariant: irrespective of the order of approximation M, the elliptic point(s) O and saddle point(s) S are invariant (for S and O, see the phase space plot in Fig. 1), and there always exists a separatrix orbit(s) going out from S and returning to S encircling O. In the region encircled by the separatrix all the orbits form a closed orbit going around O, as is seen in the phase space plot in Fig. 1. The closed orbits are quantized according to the semiclassical quantization rule of action

$$I_n \equiv \oint p(q)\, dq/2\pi = (n + 1/2)k, \quad n = 0, 1, \ldots, \lfloor n_{\rm max}\rfloor. \quad (23)$$

Here n is the quantum number and $p = p(q)$ is the classical orbit satisfying $H_{\rm eff}^{(M)}(p(q), q) = E$. Let $I_{\rm max}$ be the action of the separatrix orbit and define the maximal quantum number $n_{\rm max}$ by $(n_{\rm max} + 1/2) = I_{\rm max}$, where $n_{\rm max}$ is not in general an integer. The orbit specified by Eq. (23) with $0 \leqslant n \leqslant \lfloor n_{\rm max}\rfloor$ represents a quantized orbit classically confined inside the closed separatrix orbit. In the case of the Hénon map, the elliptic point is O:(0,0) and the saddle point is S:$(-4, 0)$, and the quantized orbit Eq. (23) leaks out toward $q = -\infty$ by the tunneling through the potential barrier on which the saddle S is sited.

In the case of the standard map, the potential is symmetric and has two identical valleys with the elliptic points O: $(-\pi, 0)$ and O:$(\pi, 0)$ at the bottoms. Each of the two valleys has the eigenstates which are semiclassical quantization of orbits according to Eq. (23). Two orbits of the same quantum number n localized in the two valleys degenerate in the small limit of k, but for finite k they are mixed by the tunneling interaction through the potential barrier to form the tunnel doublet with even and odd parity.

As in Ref. [33], we consider only the eigenstates of even parity, which have nonzero amplitude at the top of the potential barrier $q = 0$, and use the quantum number $n = 0, 1, 2, \ldots$ defined by Eq. (23) to assign the even parity states. We next consider the semiclassical tunneling process

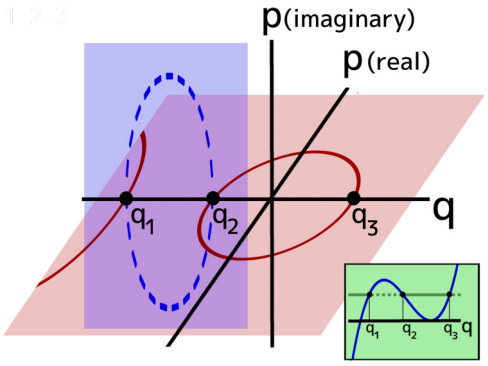

FIG. 2. The instanton orbit (blue broken curve) connecting the two real orbits (red solid curves) at their turning points q_2 and q_1. This is the case of the Hénon map having a closed real orbit (the right orbit) and an open real orbit extending toward $q = -\infty$ (the left solid curve). The insert indicates the potential energy, the system's energy, and the turning points q_1, q_2, and q_3 in the case of the lowest order Hamiltonian of Eq. (13).

of the integrable model, which is described by the imaginary orbit $p = ip_n^{(\rm ins)}(q)$; $q \in \mathbb{R}$, which is determined by the condition $H_{\rm eff}^{(M)}(ip_n^{(\rm ins)}(q), q) = E_n$. Such an imaginary orbit $p = ip_n^{(\rm ins)}(q)$ [more precisely $p = \pm ip_n^{(\rm ins)}(q)$] is called an instanton, and it is paired with the real orbit $p = \pm p_n(q)$ satisfying the same condition $H_{\rm eff}^{(M)}(p_n(q), q) = E_n$ which appeared in Eq. (23). The relation between the two kinds of orbit is illustrated in Fig. 2. The imaginary and real orbit contact with each other at its turning point, say, $q = q_2$, at which $p_n(q_2) = ip_n^{(\rm ins)}(q_2) = 0$. The instanton starts from $q = q_2$ and goes through the pure imaginary space and returns to the real world at another turning point $q = q_1$ satisfying $p_n^{(\rm ins)}(q_1) = 0$, which may be called the exit of the tunneling. At a position q taken between the two turning points q_1 and q_2 the tunneling probability is given by

$$P_{\rm tun} = \left|\left\langle q\right| u_n^{(M)}\right\rangle\right|^2 \sim e^{-2S^{(\rm ins)}(q)/k},$$
$$\text{where} \quad S^{(\rm ins)}(q) = \left|\int_q^{q_2} p^{(\rm ins)}(q)\, dq\right|. \quad (24)$$

As the representative point at which tunneling probability is observed, we take the exit $q = q_1$ for the Hénon map, and for the case of the standard map we take $q = 0$ at which the potential barrier is peaked.

The simplest example is taken from the lowest-order BHC Hamiltonian $H_{\rm eff}^{(1)}(p, q) = p^2/2 + V(q)$, for which the real and instanton orbits are $p_n(q) = \sqrt{2[E - V(q)]}$ and $p_n^{(\rm ins)}(q) = \sqrt{2[V(q) - E]}$, respectively. The turning points are decided by $V(q) = E$. In the case of the Hénon map, for example, q_1 and q_2 are the left and the middle zeros of the three roots of $V(q) = E$. The instanton tunneling rate displayed in Fig. 1 is the instanton of sufficiently high-order $H_{\rm eff}^{(M)}$, but it does not significantly depend upon M in the nearly integrable regime.

In the nearly integrable regime considered in the present paper, the quasibound states of the effective Hamiltonian $H_{\rm eff}^{(M)}$ specified by Eq. (23) approximate very well those of the original evolution operator $\hat{U}$, and so there exists a one-to-one

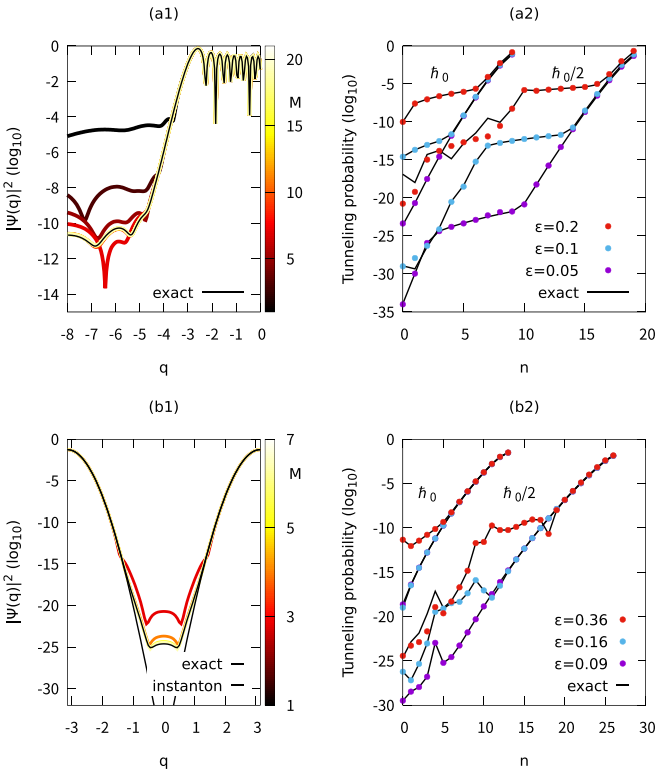

FIG. 3. Convergence of tunneling tail of eigenfunction to the exact numerical result with several M for (a1) the Hénon map and for (b1) the standard map. For $M > 7$ [for (a1)] and $M > 3$ [for (b1)] the perturbation results coincide with the exact results. The amplitude of tunneling tail of exact solution (solid line) and of perturbation theory (solid circle) is compared in (a2) the Hénon map and in (b2) the standard map at various values of ϵ. The order of approximation is $M = 15$ for (a1) and $M = 9$ for (b1). Here $\hbar_0 = 0.629\sqrt{\epsilon}$ for the Hénon map and $\hbar_0 = 0.251\sqrt{\epsilon}$ for the standard map [$\bar{k} = 0.629$ and 0.315 for (a2), and $\bar{k} = 0.251$ and 0.125 for (b2)].

correspondence between the eigenstates of $H_{\rm eff}^{(M)}$ and those of $\hat{U}$.

In the nearly integrable regime, the integrable approximation works well in quantum mechanics as well as in classical mechanics: if we confine ourselves to the classically accessible region of the coordinate q, the eigenfunction of the integrable approximation by $H_{\rm eff}^{(M)}$ agrees quite well with that of $\hat{U}$.

However, the tunneling component of wave function is significantly different even if the nonintegrability parameter ϵ is small. Indeed, Fig. 1 shows clearly that for the quantum number n less than the characteristic number n_c, the tunneling amplitude of the eigenfunction of $\hat{U}$ exhibits marked increase from that of the integrable approximation, which is approximated by the instanton formula (24),

III. RESULTS OF PERTURBATION THEORY AND INTERPRETATIONS FOR THEM

A. Results of perturbation theory

In Figs. 3(a1) and 3(b1) we show typical wave functions of eigenfunctions in the tunneling regime calculated by the lowest-order perturbation theory for the Hénon map and the standard map, respectively. For small M the residual part $\delta\hat{U}^{(M)}$ is too large to reproduce the exponentially small tunneling tail. However, the result of perturbation theory improves with M and converges to the exact tunneling tail.

In Figs. 3(a2) and 3(b2) the typical characteristic value of the tunneling probability $P_{\rm tun}$ computed respectively for the Hénon map and the standard map by the lowest-order perturbation theory are shown as a function of the quantum number n up to $n_{\rm max}$. The results are compared with those obtained by the exact numerical diagonalization. Here $P_{\rm tun}$ is defined as a square average of the modulus of the wave function in a fixed interval $\mathcal{T} = [q_a - A/2, q_a + A/2]$ of q in which the concerned eigenfunction $|u_n^{(M)}\rangle$ consists only of the tunneling component. Then

$$P_{\rm tun} = \langle\langle |\langle q|u_n\rangle|^2 \rangle\rangle, \tag{25}$$

$$\text{where} \quad \langle\langle X(q)\rangle\rangle \equiv \int_{q\in\mathcal{T}} X(q)\,dq \Big/ \int_{q\in\mathcal{T}} dq.$$

In the case of the Hénon map we take $q_a + A/2 \ll -4$, i.e., far from the exit $q = q_1$ of tunneling, and take A much larger than the wavelength, while in the case of the standard map we set $q_a = 0$ or 2π and take $A = 0$, focusing to the tunneling probability at the site of the top of the barrier, which is the center of symmetry. From Fig. 3 it is evident that the perturbation theory well reproduces the results obtained by the numerical diagonalization over a wide range of n including the I-NI transition region, if ϵ is small enough. The main features of the tunneling characteristics observed in Fig. 3 and more closely in Fig. 1 are as follows:

(1) Transition to a plateau: if the quantum number n is close to $n_{\rm max}$, the tunneling probability $P_{\rm tun}$ decreases steeply following the instanton probability, but there exists the threshold quantum number $n_c = n_c(\epsilon, \bar{k})$ at which a transition from the instanton tunneling occurs [34]. Below n_c, $P_{\rm tun}$ keeps almost the same level forming a plateau.

(2) Staircase structure: with further decrease in n, the plateau terminates at a certain n, and $P_{\rm tun}$ exhibits a steep decrease similar to the instanton region, which terminates at a certain n, and a plateau region emerges again beyond it. In short, the plateau region and the steep-decay region following it are repeated to form a staircase structure. The very similar staircase was also observed for the $1/\hbar$-dependency of the ground state ($n = 0$) tunneling rate for the standard map [33].

(3) The quantization condition says that the maximum number $n_{\rm max}$ of quasibound states increases in proportion to $1/\bar{k}$. The number of states in the instanton region $n_{\rm max} - n_c$ and the height of the first plateau do not depend on $\bar{k}$ sensitively. But they depend on ϵ very sensitively; as shown later, it exhibits an essentially singular increase with decrease in ϵ.

Therefore, by taking ϵ extremely small, the tunneling processes of all the quasibound states can be instanton processes. Then a question arises: however small ϵ may be, does the I-NI transition happen if we take the limit $\bar{k} \to 0$? This is a crucial question asking whether the instanton tunneling along the tori is always interrupted in the semiclassical limit.

Because of the success of the perturbation theory, we can now understand the quantum mechanism of the above tunneling characteristics by using the eigenstates of the higher-order integrable model $H_{\rm eff}^{(M)}$. In the next subsection,

we discuss very characteristic features of the TME and the expansion coefficient (EC) $|\langle\Psi_n|u_j^{(M)}\rangle| = R_{nj}\langle u_n^{(M)}|\delta\hat{U}^{(M)}|u_j^{(M)}\rangle|$ with respect to the eigenstates of the high-order integrable BHC Hamiltonian, which is keys to understand the tunneling characteristics.

B. Unrenormalizable invariant elements of the transition matrix and of the expansion coefficients

In the one-dimensional autonomous Hamiltonian system, it is expected that the correspondence principle can be applied to the classical evaluation of the matrix element. The matrix element of an observable $\hat{O}(p,q)$ with respect to two states of quantum number n, j, i.e., $\langle u_n^{(M)}|\hat{O}(q,p)|u_j^{(M)}\rangle$, corresponds to a Fourier component of the Weyl symbol $O_{\rm cls}(q,p)$, which is related to the position representation of the matrix element as

$$\langle q_1|\hat{O}|q_2\rangle = \frac{1}{2\pi}\int dp e^{ip(q_1-q_2)/\hbar} O_{\rm cls}[(q_1+q_2)/2, p]. \quad (26)$$

With this symbol the correspondence principle in the action-time (angle) representation is expressed as [36]

$$\left\langle u_n^{(M)}\middle|\hat{O}(\hat{p},\hat{q})\middle|u_j^{(M)}\right\rangle \sim \frac{\omega(I_{nj})}{2\pi}\int_0^{2\pi/\omega(I_{nj})} O_{\rm cls}[X(I_{nj},t)]e^{i(j-n)\omega(I_{nj})t}, \quad (27)$$

using the action $I_{nj} \equiv (I_n + I_j)/2$ and the classical frequency

$$\omega(I) = \frac{dH_{\rm eff}^{(M)}(I)}{dI}, \quad (28)$$

and the period $T(I) = 2\pi/\omega(I)$. Here we omit the superscript (M) for $\omega(I)$ and $T(I)$. Note that if the classical orbit of action I_{nj} is not close to the separatrix and $\omega(I_{nj})$ is sufficiently nonzero, then we can roughly estimate as

$$\frac{E_j - E_n}{\hbar} \simeq \frac{I_j - I_n}{\hbar}\left.\frac{dH_{\rm eff}^{(M)}(I)}{dI}\right|_{I=I_{nj}} = (j-n)\omega(I_{nj}), \quad (29)$$

which is the frequency factor of the Fourier integral of Eq. (27). If $O_{\rm cls}[X(I_{nj},t)]$ is an analytic function of X, then the poles of $O_{\rm cls}[X(I_{nj},t)]$ are decided by those of the orbit $X(I_{nj},t)$. Since the integrand of Eq. (27) is a periodic function of the period $T(I_{nj}) = 2\pi/\omega$, we can deform the integral path along the real interval $[0, T(I_{nj})]$ so as to encircle the pole in the complex domain, and Eq. (27) is evaluated as

$$\left\langle u_n^{(M)}\middle|\hat{O}(\hat{q},\hat{p})\middle|u_j^{(M)}\right\rangle \propto |j-n|^{d-1}e^{-t_s(I_{nj})\omega(I_{nj})|j-n|}, \quad (30)$$

where $t_s(I_{nj})$ is the imaginary part of the pole closest to the real axis, and d is the degree of the pole.

In Fig. 4 typical examples of the transition matrix element (TME) $\langle u_n^{(M)}|\delta\hat{U}^{(M)}|u_j^{(M)}\rangle$, which plays a key role in our perturbation theory, are shown as (i) for the Hénon map and the standard map. The corresponding expansion coefficient (EC) of the perturbed eigenfunction

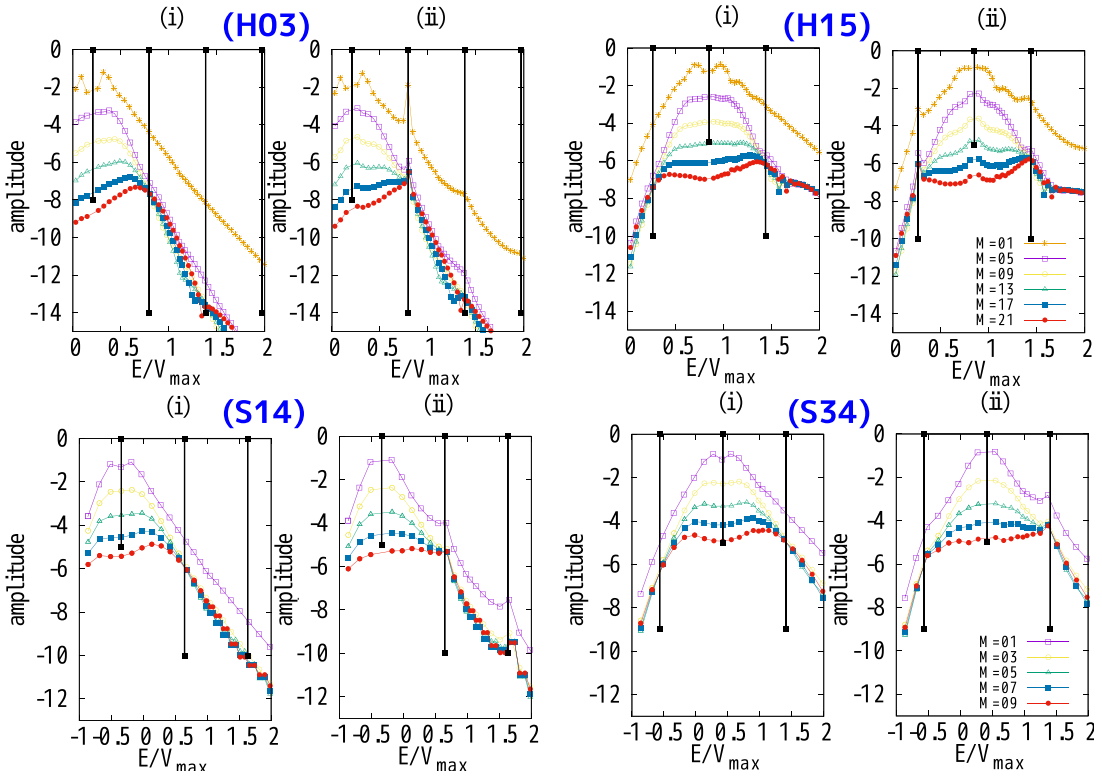

FIG. 4. M dependency of (i) the transition matrix element and (ii) the expansion coefficient, where the amplitude is shown in $\log_{10}$ and the function of eigenenergy normalized by $V_{\rm max}$. H14 and H15 are the eigenstates $n = 3$ and $n = 15$ of the Hénon map, and S14 and S34 indicate the quantum number $n = 14$ and $n = 34$ of the standard map. The vertical line ending with squares indicates E_n (shorter vertical line) and the resonant energies $E_\ell^{\rm Res}(E_n) = E_n \pm \Omega\hbar\ell$ (longer vertical lines). Note that the fixed points are located at $E_\ell^{\rm Res}(E_n)$. Here $\epsilon = 0.1$.

$\langle u_n^{(M)}|\Psi_n^{(M)}\rangle = \langle u_n^{(M)}|\delta\hat{U}^{(M)}|u_j^{(M)}\rangle R_{nj}^{(M)}$ is also shown as (ii), where n is chosen as representative states. The difference between TME and EC is only the resonance factor $R_{nj}^{(M)}$, which is very insensitive to M and brings about only a numerical correction of $O(1)$ except for the exact resonance.

For small M, the TME $|\langle u_n^{(M)}|\delta\hat{U}^{(M)}|u_j^{(M)}\rangle|$ exhibits a simple exponential decay with the energy difference $|E_n - E_j|$ as indicated by Eq. (30), which seems to be a quite natural behavior. As M increases, such a behavior markedly changes in the modes around the diagonal mode. For large M, $\|\delta\hat{U}^{(M)}\|$ decays in general following Eq. (19), but the modulus of TME is invariant against M at the specific energy $E = E_1^{\mathrm{Res}}(E_n)$, where

$$E_1^{\mathrm{Res}}(E_n) = E_n + \Omega\hbar. \tag{31}$$

As can be observed in Fig. 4(i), the TME forms a broad peak around $E_1^{\mathrm{Res}}(E_n)$. This specific energy has a clear physical meaning: it is the energy separated from E_n by the fundamental quantum (12) decided by the period of the quantum map. This strongly suggests the occurrence of quantum resonance with the periodic kick of the quantum map. The EC $|\langle\Psi_n^{(M)}|u_j^{(M)}\rangle|$ is the product of the TME $|\langle u_n^{(M)}|\delta\hat{U}^{(M)}|u_j^{(M)}\rangle|$ and the resonant factor $R_{nj}^{(M)} \sim O(1)$, and so it is dominated by the broad resonance peak of the TME as is indicated by Fig. 4. In addition, the resonance factor diverges at the exact resonance $E = E_1^{\mathrm{Res}}(E_n)$. It reinforces the coupling with a closely resonant mode among the modes in the broad resonance peak of TME. Hence EC also forms a broad resonance peak, and its peak shape is more pronounced than that of TME with an invariant peak height as is displayed in Fig. 4(ii).

The TME is a matrix element of the evolution operator defined for a *finite* time evolution, and so the quantum resonance leads to an enhancement of its amplitude proportional to the timescale, but the EC is a component of the energy eigenstate determined over an *infinite* timescale, and it has divergently large amplitude at the exact resonance. Such features are reflected in the difference between TMC and EC very close to the resonance. The enhancement of TME around the quantum resonance will be discussed in connection with the classical nonlinear resonance in Appendix D.

The presence of peaks in TME can be observed also at the higher harmonic energies

$$E_\ell^{\mathrm{Res}}(E_n) = E_n + \ell\Omega\hbar, \quad \text{where } \ell = 1, 2, \ldots, \tag{32}$$

which are more evidently pronounced in the ECs. The peak heights there are also invariant against the increase of M. The above facts imply quite an important feature of the quantum map systems: no matter how large M may be, the BCH transformation cannot renormalize particular components of the off-diagonal elements of the evolution operator as the integrable evolution operator. The unrenormalizable components remain invariant with respect to the increase of M and finally form broad resonance peaks around the resonant energies $E = E_\ell^{\mathrm{Res}}(E_n)$. In short, the BHC transformation cannot renormalize the periodic perturbation inherent in the quantum map as the effective integrable Hamiltonian $H_{\mathrm{eff}}^{(M)}$, and its unrenormalizable elements remain as the invariant broad peak.

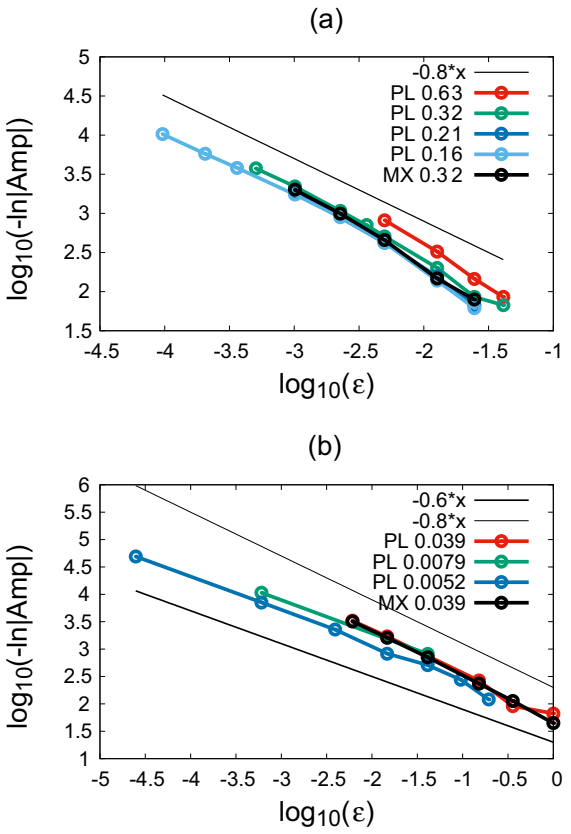

FIG. 5. The black and colored curves with points represent the ϵ dependency of $\log_{10}(-\ln P_1)$ for the different $\hbar$, where P_1 is the invariant resonance peak height of EC, (a) for the Hénon map and (b) for the standard map. The colored curves (except for the black curve) are evaluated by using tunneling amplitude of the first plateau in Fig. 1, because the numerical evaluation of P_1 becomes harder as $\hbar$ gets smaller. MX means that P_1 is determined by the peak height of EC at the plateau edge, and PL by the tunneling amplitude of the plateau.

On the other hand, another notable feature of the invariant broad peaks is that its peak height exhibits a quite singular nature; it depends on the parameter ϵ in an essentially singular way. Moreover, as is shown later, the invariant broad peak is quasiclassical in the sense that its height is insensitive to the Planck constant $\hbar$. The peak height of EC with respect to the TME peak mode also has the same nature because the resonant factor R_{nj} results in only a numerical correction. In fact, taking the eigenstate of $n = n_{\mathrm{edge}}$ at the "edge" of the plateau as the typical eigenstate of the plateau (its precise definition is given later) the broad invariant peak height of the EC, which we denote by P_1, is shown in Fig. 5(b). It is not sensitively dependent upon $\hbar$. As shown in Fig. 5, however, it exhibits an essentially singular ϵ-dependence as

$$P_1 \sim C_0 e^{-C_1\epsilon^{-\alpha}}, \tag{33}$$

where C_0, C_1 are constants and the exponent α takes 0.7–0.8 for the Hénon map and ~0.6 for the standard map. Here we take a very specific state of $n = n_{\mathrm{edge}}$, but the peak height of the modes satisfying the condition (32) does not sensitively change with n. It is numerically not so easy to obtain P_1

directly from the TME and EC, but, as will be discussed later, it can be replaced by the tunneling amplitude of the plateau just after the I-NI transition, shown in Fig. 5.

As shown in Eq. (33), the singular dependence upon the nonintegrability parameter ϵ reminds us of the Melnikov integral characterizing the separatrix splitting, which measures classical chaos of the nearly integrable system. The relationship with the Melnikov integral will be argued in the next section and Appendix A on the basis of the correspondence principle Eq. (27).

In addition, we numerically confirmed that the peak height P_ℓ at the higher harmonic energy is related to P_1 simply by

$$P_\ell \sim P_1^\ell. \tag{34}$$

Thus, the higher harmonic peaks are also "infected" with the singular property of the first massive peak.

In summary, the magnitudes of TME and EC decrease markedly with increase in M except for the resonance region $E \sim E_n \pm \hbar\Omega$, in which a broad peak whose height is invariant against M remains. The broad peak of EC is more definitely peaked than that of TME by the enhancement of quantum resonance factor. The height of this broad resonance peak is insensitive to $\hbar$ and exhibits an essentially singular dependence on ϵ like $e^{-\text{const.}\epsilon^{-\alpha}}$ (const > 0, $0 < \alpha < 1$) if the mode has energy not far from $V_{\max}$. The TME and EC decay almost exponentially beyond the broad resonance peak, but they also have the M-invariant local peaks around the higher harmonic locations $|E - E_n| \sim$ integer $\times\, \Omega\hbar$.

C. Contribution spectrum, tunneling characteristics, and singular invariant peak

In this section we first show that renormalization-invariant elements of the TME and EC of the high-order M discussed in the previous section are directly reflected in the I-NI transition and the tunneling characteristics beyond the transition. We introduce the *contribution spectrum* [33,34] which measures the contribution to the tunneling tail from each eigenstate $|u_j^{(M)}\rangle$:

$$\text{Con}^M_{j\to n} \equiv \langle\langle |\langle q|u_j^{(M)}\rangle|^2\rangle\rangle |\langle u_j^{(M)}|\psi_n^{(M)}\rangle|^2, \tag{35}$$

where the $\langle\langle\cdot\rangle\rangle$ is the local average defined in Eq. (25). We call $\text{Con}^M_{j\to n}$ versus j the contribution spectrum. Here we assume that the order M is large enough such that the lowest perturbation calculation well reproduces exact ones, and then the contribution spectrum is expressed as

$$\text{Con}^M_{j\to n} = \begin{cases} \langle\langle |\langle q|u_n^{(M)}\rangle|^2\rangle\rangle & (j=n), \\ \langle\langle |\langle q|u_j^{(M)}\rangle|^2\rangle\rangle |\langle u_j^{(M)}|\delta\hat{U}^{(M)}|u_n^{(M)}\rangle|^2 |R_{nj}^{(M)}|^2 & (j\neq n). \end{cases} \tag{36}$$

The diagonal term $j = n$ represents the tunneling component of the unperturbed eigenfunction, and so it represents the instanton component. Unless the exact resonance condition is accidentally satisfied, the resonance factor $R_{nj}^{(M)} = 1/(e^{-i\frac{\sqrt{\epsilon}}{\hbar}E_n} - e^{-i\frac{\sqrt{\epsilon}}{\hbar}E_j})$ is $O(1)$ and it may be neglected.

Decomposition into the contribution spectrum enables us to extract predominant modes. However, it should particularly be remarked that sufficiently high-order integrable basis $|u_j^{(M)}\rangle$ of $H_{\text{eff}}^{(M)}$ must be used for the contribution spectrum analysis. If a lower order basis is employed, a number of components such that $\text{Con}^M_{j\to n} \gg \langle\langle |\langle q|\psi_n^{(M)}\rangle|^2\rangle\rangle$ appear and the perturbation theory breaks down.

Even though the perturbation theory works well for sufficiently large M, the most dominant component in the contribution spectrum typically overestimates the exact tunneling amplitude, which implies that a cancellation among the predominant components occurs and extracting the maximal component does not make sense, as is seen in the Hénon map (see Appendix B). Roughly speaking, the condition that the contribution spectrum analysis is meaningful is

$$\text{Max}\{\text{Con}^M_{j\to n}\} \sim \text{actual tunneling amplitude}. \tag{37}$$

First, we consider the instanton component of the BHC eigenstates $u_n^{(M)}(q)$, which is nothing but $\text{Con}^M_{n\to n}$. It is convenient to measure the semiclassical quantities such as energy, action, and quantum number, by taking the classical separatrix orbit on the top of the barrier as the origin. Let $V_{\max} = H_{\text{eff}}^{(M)}(\text{S})$ be the energy at the saddle S and take the action and quantum number of the separatrix orbit, i.e., $I_{\max}$, $n_{\max}$ $(= I_{\max}/\hbar - 1/2)$ as the origins. Then we introduce

$$\begin{aligned} \delta I_n &= I_{\max} - I_n, \quad \delta n = n_{\max} - n, \\ \delta E_n &= V_{\max} - E_n. \end{aligned} \tag{38}$$

We briefly discuss some general properties of the states near the top of potential. Let us first consider the relationship between δn and the energy δE. As $\delta E \to 0$, the classical orbit approaches to the separatrix orbit. Then the period of the orbit, which is related to the orbital frequency (28) by $T(\delta E) = 2\pi/\omega(\delta E)$, diverges logarithmically and is in general expressed as

$$\frac{d\delta I}{d\delta E} = \frac{1}{\omega(\delta E)} \sim -A_0 \ln(\delta E) + A_1 + O(\delta E), \tag{39}$$

where A_0 and A_1 are positive constants. Integrating both sides, we obtain

$$\delta n = \nu\left(\frac{\delta E_n}{\hbar}\right)\frac{\delta E_n}{\hbar}, \tag{40}$$

where

$$\nu(x) := -A_0 \ln x + (A_1 + A_0 - A_0 \ln\hbar) + O(\hbar x). \tag{41}$$

Thus, δn increases with $\frac{\delta E}{\hbar}$ weakly depending upon $\hbar$ through $\ln\hbar$.

Next we evaluate the action $S^{(\text{ins})}(I) := S^{(\text{ins})}(q_1)$ of an imaginary orbit, i.e., the instanton contacting with the closed real orbit with the action I. We suppose the real orbit representing the bound state is close to the potential barrier. The lowest-order Hamiltonian (13) suffices for our purpose. Let $q_{\max}$ be the q at which the potential $V(q)$ has a local maximum ($q_{\max} = -4$ for the Hénon map and $q_{\max} = 0$ or 2π for the standard map), then the instanton orbit is approximated by $p^2/2 = \delta E - \omega_{\text{top}}^2(q - q_{max})^2/2$ where $\omega_{\text{top}}^2 = V''(q_{\max}) \sim O(1)$. This gives the instanton action $2S^{(\text{ins})}(I) = \delta E/\omega_{\text{top}}$ from Eq. (24) and

$$\langle\langle |\langle q|u_n^{(M)}\rangle|^2\rangle\rangle \sim e^{-2\frac{S^{(\text{ins})}(I_n)}{\hbar}} = e^{-\frac{\delta E_n}{\omega_{\text{top}}\hbar}}. \tag{42}$$

Note again that the contribution spectrum has the principal component at $j = n$ with amplitude $\langle\langle|\langle q|u_n^{(M)}\rangle|^2\rangle\rangle$, which is equal to the instanton probability (42) of the mode n. On the other hand, the second peak in the TME is the broad resonance peak located at the quantum resonance $E_j \sim E_1^{\rm Res}(E_n) = E_n + \hbar\Omega$. If n is close to $n_{\max}$, then $E_1^{\rm Res}(E_n) > V_{\max}$ and the channel j with the energy around $E_1^{\rm Res}(E_n)$ is not bound by the potential barrier but extends beyond it, which means the probability behaves as $\langle\langle|\langle q|u_j^{(M)}\rangle|^2\rangle\rangle \sim O(1)$. Thus, $\mathrm{Con}_{j\to n}^M$ has a second peak at the modes in the first broad resonance $E \sim E_1^{\rm Res}(E_n)$ and its height is estimated by Eq. (33). The instanton contribution at $j = n$ and the peak modes with the energy eigenvalues $E_j \sim E_1^{\rm Res}(E_n)$ are thus compete.

Since $R_{nj} \sim O(1)$ in Eq. (36), we evaluate this as

$$\frac{\text{1st resonance peak contribution}}{\text{instanton}} \sim \frac{C_0^2 e^{-2C_1\epsilon^{-\alpha}}}{e^{-\frac{\delta E_n}{\omega_{\rm top}\hbar}}}, \tag{43}$$

by using Eqs. (42) and (33). If ϵ is small enough, this numerator is extremely small, whereas the denominator is not small unless n is far from $n_{\max}$ and $\frac{\delta E_n}{\hbar} \ll \omega_{\rm top}$. In that case, the instanton contribution always exceeds the broad resonance peak modes. However, as n reduces further from $n_{\max}$, the instanton action $\propto \frac{\delta E_n}{\omega_{\rm top}}$ increases, and at the critical energy $E_C = E_n$ satisfying

$$\frac{\delta E_C}{\hbar} \sim \omega_{\rm top} C_1 \epsilon^{-\alpha}, \tag{44}$$

the contribution from the broad resonance peak dominates the instanton contribution. This is exactly the instanton-noninstanton (I-NI) transition seen in Fig. 1. By Eq. (40), $\delta E_C/\hbar$ may be read as the number of the states δn_c exhibiting the instanton tunneling, which is insensitive to $\hbar$, as is confirmed numerically with Fig. 1. If n satisfies the condition $E_{n1}^{\rm Res}(E_n) = E_n + \hbar\Omega > V_{\max}$, the amplitudes of the modes around $E_{n1}^{\rm Res}(E_n)$ are not bound and so $\langle\langle|\langle q|u_j^{(M)}\rangle|^2\rangle\rangle \sim O(1)$. Thus, the largest contribution is due to the first resonance peak mode at $E_j \sim E_{n1}^{\rm Res}$. Moreover TME peak keeps the value given by the estimation of Eq. (33), which is given by

$$P_{\rm tun} \sim P_1^2 = C_0^2 e^{-2C_1\epsilon^{-\alpha}}, \tag{45}$$

and it forms the plateau observed in the tunneling characteristics immediately after the I-NI transition, and the plateau height can be identified with the peak intensity P_1. This fact was used for plotting the P_1 versus ϵ plot shown in Fig. 5. We stress again that the plateau height is not very sensitive to $\hbar$, as is suggested by Figs. 1 and 3, and is closely shown by the summarized results in Fig. 5

As n decreases further and becomes less than the quantum number $n_{\rm edge}$, which is defined by

$$E_1^{\rm Res}(n_{\rm edge}) < V_{\max} \leqslant E_1^{\rm Res}(n_{\rm edge}+1), \ \text{i.e.,} \ \delta E_n \sim \Omega\hbar, \tag{46}$$

the resonance peak mode becomes an eigenstate of $E_j < V_{\max}$ bound by the barrier, and the average probability $\langle\langle|\langle q|u_j^{(M)}\rangle|^2\rangle\rangle$ is now replaced by the instanton probability of the quasibound state, which is evaluated with replacing δE_n by $\delta E_j = \delta E_n + \Omega\hbar$ in Eq. (24). Since the peak intensity P_1 does not sensitively depend upon n as was remarked in the previous section, the tunneling probability steeply decreases with n, according to the instanton probability:

$$P_{\rm tun} \sim P_1^2 e^{+\frac{\Omega}{\omega_{\rm top}}} e^{-\frac{\delta E_n}{\omega_{\rm top}\hbar}}. \tag{47}$$

This is the steep-slope region, and the quantum number $n_{\rm edge}$, which was used in the previous subsection, has a definite meaning by Eq. (46). Thus, at the quantum number $n_{\rm edge}$ the tunneling characteristic changes from the plateau to the steep slope. We further note that δn_c and $\delta n_{\rm edge}$ do not strongly depend upon $\hbar$, as is suggested by Fig. 1. This can be explained from the fact that the $\delta E_n/\hbar$ for the states $n = n_c$ and $n = n_{\rm edge}$ do not depend upon $\hbar$ from Eq. (44) and (46), respectively, and the relation between δn and δE given by Eq. (40)

In the steep-slope region, the resonance broad peak of EC with the height P_1 is responsible for the tunneling. Here we consider the local peak of EC at the second resonance $E_j \sim E_2^{\rm Res}(E_n)$ with the height $P_2 \sim P_1^2$ [see Eq. (34)]. Such a mode has energy greater than $V_{\max}$ and so $\langle\langle|\langle u_j^{(M)}|q\rangle|^2\rangle\rangle \sim O(1)$, and the contribution $\mathrm{Con}_{j\to n}^M$ is decided by $P_2^2 \sim P_1^4$ [see Eq. (34)]. Hence the ratio of the second resonance peak contribution to the first resonance peak one is

$$\frac{\text{2nd resonance peak contribution}}{\text{1st resonance peak contribution}} \sim \frac{C_0^2 e^{-2C_1\epsilon^{-\alpha}}}{e^{-\frac{\delta E_n - \hbar\Omega}{\hbar\omega_{\rm top}}}}, \tag{48}$$

which repeats the same variation of the ratio shown by Eq. (43) in the pretransitional regime. This fact implies the possibility that the same kind of transition as the I-NI transition is repeated again between the first and second peaks as $\delta E_n - \Omega\hbar$ increases further. However, in order that the scenario mentioned above holds, the contribution spectrum should really have a predominant contribution around the second peak position of EC. This issue will be clarified in Sec. III E.

D. The singular invariant peak

Here we present a possible explanation of the singular dependency of the NI tunneling probability upon ϵ represented by Eq. (33) by using the correspondence principle. The edge state $|u_{n_{\rm edge}}^{(M)}\rangle$ suits our purpose: it is at the border between the plateau and the steep-slope region, and so it has the tunneling probability P_1^2, whereas its first resonance mode $|u_j^{(M)}\rangle$ having the resonance energy $E_1^{\rm Res}(E_n) = E_n + \Omega\hbar$ can be taken as the quasibound state with the energy just below $V_{\max}$, and then the correspondence principle is applicable to the TME between the two quasibound states $|u_j^{(M)}\rangle$ and $|u_n^{(M)}\rangle$.

P_1 can be identified with the modulus of TME $\langle u_{n_{\rm edge}}^{(M)}|\delta\hat{U}^{(M)}|u_j^{(M)}\rangle$. Then we can set $\delta E_n = V_{\max} - E_n \sim \Omega\hbar$, and the effective frequency of the exponential function in the Fourier integral of Eq. (27), i.e., $\Omega_{\rm eff} := (j-n)\omega(I_{nj})$, where $j = n_{\max}$, can be rewritten by using Eq. (40),

$$\delta n := n_{\max} - n \sim (-A_0 \ln|\Omega\hbar| + A_1 + A_0)\Omega, \tag{49}$$

and Eq. (39) as

$$\Omega_{\rm eff} = \delta n\omega(\delta I_n/2) = r\Omega, \tag{50}$$

where

$$r = [\omega(\delta I_n)^{-1} + A_0 + O(\Omega\hbar)]\omega(\delta I_n/2). \tag{51}$$

Here the physical quantities are regarded as the functions of either $\delta I_n = \delta n\hbar$ or δE_n. We are interested in the semiclassical limit $\hbar \ll 1$ and $\delta E_n = \Omega\hbar(\ll 1)$. Then the energy $H_{\rm eff}^{(M)}(\delta I_n/2)$ approaches $V_{\rm max}$ and the classical orbit $X(\delta I_n/2, t)$ is well approximated by the separatrix orbit $X_{\rm spx}(t)$, which emanates from the saddle S and reaches itself (the Hénon map) or an another saddle (the standard map) over an infinite time. Thus $\omega(\delta I_n/2)$ and $\omega(\delta I_n)$ go to 0, which means that the parameter r asymptotically approaches the frequency ratio $\omega(\delta I_n)/\omega(\delta I_n/2)$. It does not converge to a finite value: as is shown in Appendix A, it is less than 1 and is a slowly varying function of $\Omega\hbar$, depending upon $\ln \Omega\hbar$, $\ln(\ln \Omega\hbar)$, …. Then Eq. (27) is represented as

$$P_1 \sim \left| \frac{1}{T(\delta I_n/2)} \int_{-\infty}^{+\infty} e^{ir\Omega t} \delta\hat{U}_{\rm cls}^{(M)}[X_{\rm spx}(t)]\, dt \right|. \tag{52}$$

The integral can be evaluated by using the pole of the separatrix orbit.

Since the height of TME at resonance is invariant against M, $\delta\hat{U}_{\rm cls}^{(M)}$ of a lower order M is available for the evaluation of Eq. (52). For lower M, we can expect that $\delta\hat{U}_{\rm cls}^{(M)}(X)$ is simple and is free from a singularity as a function of X, and the singularity of the integrand of Eq. (52) comes from the pole of the separatrix orbit $X_{\rm spx}(t)$. Then it can be evaluated as

$$P_1 \propto e^{-r\Omega t_s} = e^{-2\pi r t_s \epsilon^{-1/2}}, \tag{53}$$

where $t_s \sim O(1)$ is the imaginary part of the pole of the separatrix orbit closest to the real axis. The expression Eq. (53) explains the singular behavior of Eq. (45), especially for the standard map. In the case of the Hénon map the observed exponent $\alpha \sim 0.7$ is slightly larger than $1/2$, but Fig. 5 shows a strong tendency that α reduces gradually with decrease in ϵ.

A very important fact to be remarked is that the integral (52) and its result (53) as well are very similar to the Melnikov integral, which is the work done by the additionally applied oscillatory perturbation along the separatrix orbit and measures the splitting of unstable and stable manifolds [4]. It is quite implicative that the unrenormalizable invariant perturbation has an amplitude very similar to the Melnikov integral.

E. Tunneling characteristics: The multiquanta excitation processes

The I-NI transition and the following plateau region can be explained simply by the contribution spectrum analysis for both the Hénon map and the standard maps. But the contribution spectrum analysis is too rough in the sense that it considers only the modulus of contribution. Indeed, for some classes of quantum maps including open systems such as the Hénon map, the contribution spectrum analysis is not useful as a tool for analyzing the tunneling characteristics, particularly in the energy region below the first plateau. On the other hand, the analysis is very effective for closed systems such as the standard map. However, the assertion claimed for the standard map is also applicable to the Hénon map, which will be confirmed qualitatively in subsection F and quantitatively in Appendix B.

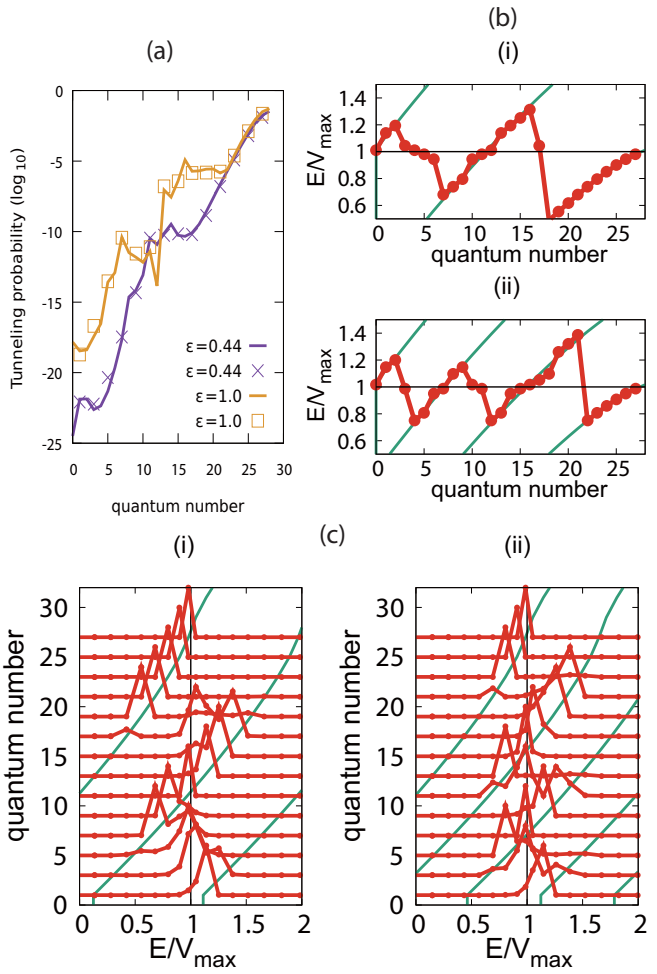

FIG. 6. (a) The comparison with the exact tunneling probability (solid line) and the most contributing mode (square and cross) for $\epsilon = 1.0$ and 0.44. (b) The energy eigenvalue of the most contributing mode plotted as the function of the quantum number n (line with points) is compared with the harmonic resonance lines $E_\ell^{\rm Res}(n)$, $\ell = 1, 2, 3$ (solid lines), where (i) $\epsilon = 0.44$ and (ii) $\epsilon = 1.0$. (c) The contribution spectrums for all the quasibound states of quantum number $0 \leqslant n \leqslant n_{\rm max}$. The spectrum is expressed as the function of normalized energy $E/V_{\rm max}$ and the solid lines indicate the location of the ℓth resonance $E_\ell^{\rm Res}(n)$ for $\ell = 0, 1, 2$, and 3.

Figure 6(a) shows the tunneling probability calculated by taking only the most dominant mode of the contribution spectrum into account. One can see that the tunneling characteristic features exhibited by the staircase structure are fully recovered. Using a high-order BHC basis, a group of mainly contributory modes are selected. The first reason explaining why it works well is the formation of the invariant broad peak of TME around the resonance energy, implying the presence of the elements unrenormalizable as the integrable Hamiltonian. Moreover, in the case of the standard map, the resonance factor is sharp enough to select more contributory modes out of many modes forming the broad resonance peak.

To simplify the problem, we pay attention to the most dominantly contributing mode as the representative mode, but the broadness of the peak of the TME and EC is very important because not only one but a number of modes in

the broad peak substantially contribute and interfere with each other to form the tunneling tail. Contribution of many modes in the broad peak is more crucial in the case of the Hénon map (see the next section and Appendix B).

In Figs. 6(b) and 6(c) the variation of the contribution spectrum and of the energy of the most contributing mode is shown, respectively, with the change of the quantum number n. The location of its energy E_n and the associated resonant harmonic energies $E_\ell^{\rm Res}(E_n)$ for $0 \leqslant \ell \leqslant 4$ are also plotted. As is evident in Figs. 6(b) and 6(c), with the decrease in n (and E_n), the maximal contribution mode changes from itself to the mode close to its first resonance energy $E_1^{\rm Res}(E_n)$, which is larger than $V_{\rm max}$, and so the responsible mode extends beyond the potential barrier. This is the I-NI transition discussed in Appendix B. As long as the condition $E_1^{\rm Res}(E_n) > V_{\rm max}$ is satisfied, the most contributing mode is the wave function unbound by the potential barrier, and it contributes to the formation of the plateau $E_1^{\rm Res}(E_n) < V_{\rm max}$, the most contributing mode is localized inside of the potential valley, and its tunneling probability, i.e., the instanton probability, for the energy $E = E_1^{\rm Res}(E_n)$ dominates again. Thus, the tunneling probability at n is $P_1 \times$ [instanton probability], which decays steeply with decrease in n and forms the steep slope region.

As n (and E_n) decreases further, the contribution from the mode in the vicinity of the second harmonic resonance $E_2^{\rm Res}(E_n)$, which is again a wave function unbound by the potential barrier, begins to grow up and exceeds the first one's contribution, and the second transition from the first-harmonic resonance to the second one eventually happens, as is clearly seen in Fig. 6(c). Thus, the process leading the tunneling mechanism changes from the single-quanta absorption process (Ωk) to the two-quanta absorption process ($2\Omega k$). The second plateau is formed immediately after the transition, which is taken the place of by the second steep slope as E_n decreases in such a way that $E_2^{\rm Res}(E_n) < V_{\rm max}$. As is seen in Figs. 6(b) and 6(c), the successive transitions are observed up to the third order. Thus, the I-NI transition and the staircase structure following it are clearly explained by the competition among the processes of *excitation by the multiquanta absorption*. We stress that the selection is caused by the broad peak of the TME and EC, which remains invariant against higher-order renormalizations, and a group of modes in the broad peak contributes to the above mechanism.

Here we briefly discuss the so-called RAT approach in comparison with our approach. The RAT approach provides a classical interpretation for the enhancement of the NI tunneling rate. The RAT interpretation is based upon an effective Hamiltonian constructed using classical information. This is in sharp contrast with our approach. We stress that the multiple-quanta excitation process deduced from the characteristic feature of exact quantum TME. Our explanation based on the multiple-quanta excitation process simply and comprehensively explains the existence of the entire staircase structure. Each step of the staircase starts with the formation of a plateau region, which is caused by the switch from resonance with the modes inside of the separatrix to resonance with the modes outside of the separatrix [33,34]. Note that the RAT approach does not take into account the modes outside of the separatrix because of its theoretical foundation. There is one more important finding in our observations in relation to the RAT theory. As shown in Fig. 4, many modes of comparable magnitude appear in the TME, while the RAT prescription considers only limited numbers of modes associated with visible classical nonlinear resonances. This subject will be discussed in more detail in Appendix D.

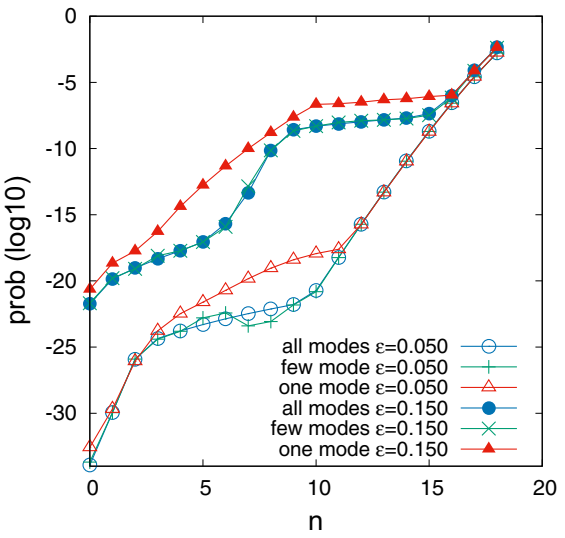

FIG. 7. The tunneling probability computed by taking only the maximally contributing mode is compared with the results obtained by taking all modes. The former is excessively larger than the latter for all n in noninstanton regime. The tunneling probability constructed by the optimal few modes prediction $\psi_n^{(M),k_{\rm max},{\rm few}}(q)$ ($k_{\rm max} = 7$) is also compared, but it almost coincides with the results of all the modes being taken into account.

F. The phase space image: The case of the Hénon map

Then how is the case of the Hénon map? In Fig. 7 we compare the tunneling probability of the one-mode approximation taking only the most contributing mode in Eq. (20) with the one for which the all modes are taken into account. It corresponds to Fig. 6(a) of the standard map. The one-mode construction can reproduce the I-NI transition and the entrance of the plateau region, but beyond it the former prediction is a few orders of magnitude larger than that of the precise result. In particular the former cannot reproduce the staircase structure anymore. Indeed, the maximal component in the contribution spectrum takes an excessively larger value than the true tunneling probability,

However, we here suppose that it is possible to extract a few number of modes from the predominant modes to reproduce the quantitative feature of the tunneling component. If this hypothesis makes sense, it turns out that only a limited number of modes substantially contribute in the tunneling region.

Now we consider the subspace spanned only by the $k_{\rm max}$ modes $\{|u_{j_1}^{(M)}\rangle, |u_{j_2}^{(M)}\rangle, \ldots, |u_{j_{k_{\rm max}}}^{(M)}\rangle\}$ and take the projection of the exact eigenfunction onto it:

$$\psi_n^{(M),k_{\rm max},{\rm few}}(q) = \sum_{k=1}^{k_{\rm max}} \langle u_{j_k}^{(M)} | \psi_n^{(M)} \rangle u_{j_k}^{(M)}(q). \qquad (54)$$

We choose the optimal set $(j_1^*, j_2^*, \ldots, j_{k\max}^*)$, where $j_1^* < j_2^* \cdots < j_{k_{\max}}^*$, such that the mean error of $\psi_n^{(M),k_{\max},\mathrm{few}}(q)$ from the exact eigenfunction

$$\mathrm{Err}(j_1, j_2, \ldots, j_{k_{\max}}) = \left\langle\!\left\langle \left| \psi_n^{(M)}(q) - \psi_n^{(M),k_{\max},\mathrm{few}}(q) \right| \right\rangle\!\right\rangle, \tag{55}$$

in the tunneling region $\mathcal{T}$ is minimal, where the optimal set is chosen among the modes exhibiting the contribution rate greater than a properly given threshold. Such is always possible if we take $k_{\max}$ sufficiently large. But we choose $k_{\max}$ as small as possible so as to cut down the wasteful components which may be dominating in the contribution spectrum but cancel after taking summation.

In fact, we show in Fig. 7 the optimal wave function $\psi_n^{(M),k_{\max},\mathrm{few}}(q)$, and taking $k_{\max} = 7$, for example, well reproduces the staircase structure of the tunneling probability as well as the plateau and steep-slope regions. In this way we can extract the most effective components forming the tunneling component.

In Appendix B, we show quantitatively that the origin of the staircase structure of the Hénon map is the multiple-quanta excitation processes and the competition among them in the same way as is described in the previous section for the standard map. In this section we observe the phase space structure of $\psi_n^{(M),k_{\max},\mathrm{few}}(q)$ by the Husimi plot and qualitatively demonstrate that the same scenario as the standard map holds in the case of the Hénon map.

In Fig. 8 a typical example of the tunneling staircase structure composed of two plateaus and one steep-slope region, which is obtained for the Hénon map $\epsilon = 0.15$, is shown. The Husimi plots of the truncated wave functions $\psi_n^{(M),k_{\max},\mathrm{few}}(q)$ with $k_{\max} = 7$ are also shown for some states representing the characteristic regions, namely, the end of the instanton region just before the I-NI transition ($n = 16$), the center of plateau after the I-NI transition ($n = 12$), the edge of the first plateau ($n = 9$), the center of the steep-slope region ($n = 7$), the end of the steep-slope region ($n = 6$), and the edge of the second plateau region ($n = 1$). Following the previous subsection, the mode responsible for the tunneling of the eigenfunction in the ℓth plateau or in the ℓth steep-slope

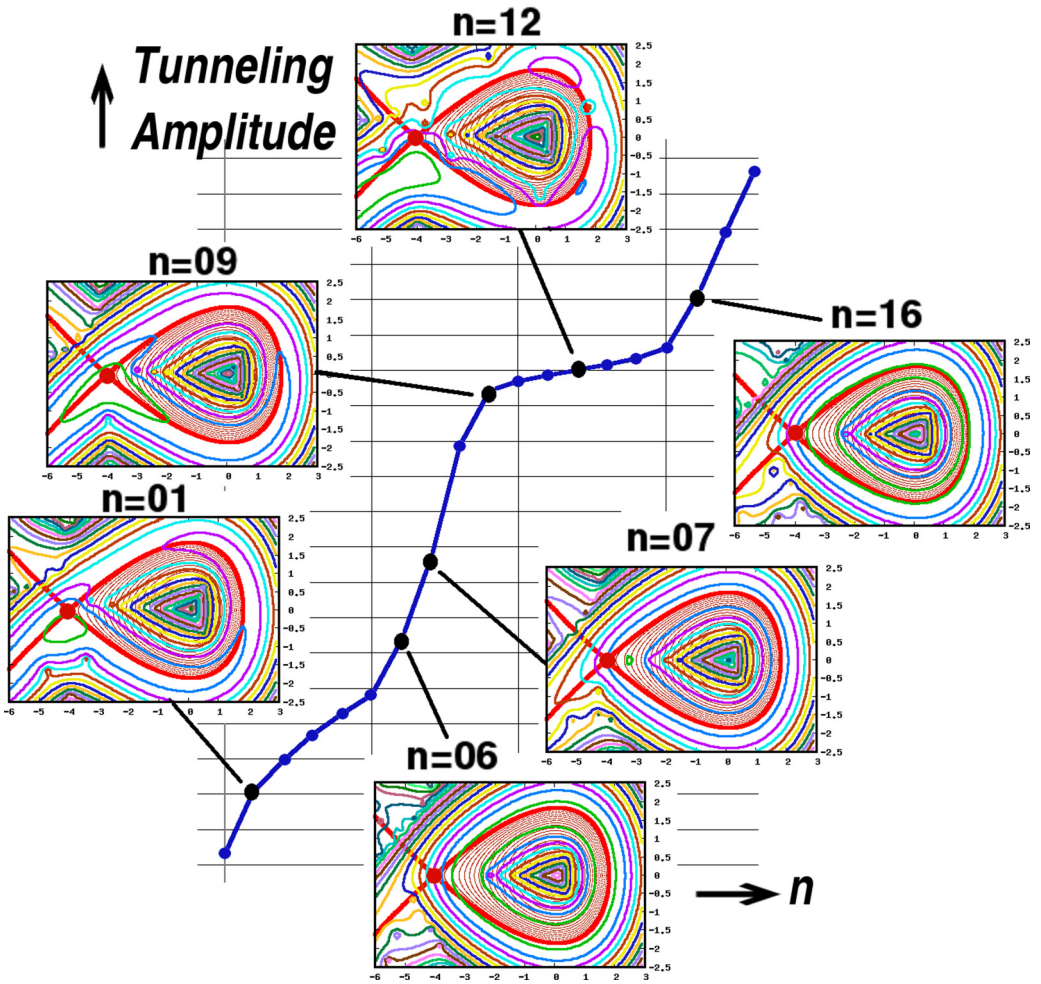

FIG. 8. The case of the Hénon map for $\epsilon = 0.15$ and $\hbar = h_0/2$ ($\bar{\hbar} = 0.32$). Along the tunneling amplitude curve, the Husimi plots of $\psi_n^{(M),k_{\max},\mathrm{few}}(q)$ are shown for the three states representing the instanton region ($n = 16$), the steep-slope regions ($n = 07, 06$) (the lower three insets), and the three states in the plateaus ($n = 12, 09, 01$) (the upper three insets). In the Husimi plot, the horizontal and vertical axes represent p and q, respectively, and the red circle indicates the saddle point $(-4, 0)$. The bold red curve passing the saddle is the stable-unstable manifolds. See the text and compare this figure with Fig. 9.

region is the mode close to the ℓth-order resonance energy $E_\ell^{\mathrm{Res}}(E_n) = E_n + \ell\hbar\Omega$. If the state is in the steep-slope region, and $E_\ell^{\mathrm{Res}}(E_n) < V_{\max}$ holds, the tunneling tail is contributed by the bound state localized inside of the separatrix. On the other hand, if the state is in the plateau, the mode responsible for the tunneling tail is the one extending outside of the separatrix. Indeed, the Husimi plots of the wave functions $\psi_n^{(M),k_{\max},\mathrm{few}}(q)$ for $n = 7$ and 6 depicted in Fig. 8 show the typical patterns of the bound eigenfunctions, which have their major distribution along the quantized classical closed orbit of the one-dimensional integrable Hamiltonian satisfying $H_{\mathrm{eff}}^{(M)}(p, q) = E_\ell^{\mathrm{Res}}(E_n)$. Further, it should be also remarked that the state $n = 16$ happens to be close to the first resonance of the state $n = 6$, that is, $E_{\ell=1}^{\mathrm{Res}}(E_6) \sim E_{16}$ and so the Husimi plot of $\psi_{n=16}^{(M),k_{\max},\mathrm{few}}$ should coincide with that of $\psi_{n=6}^{(M),k_{\max},\mathrm{few}}$, which is obviously confirmed by the Husimi plots of Fig. 8.

On the other hand, the tunneling components of the three states belonging to the plateaus region, i.e., the center of the first plateau ($n = 12$) and the edges of the first and second plateaus ($n = 9$ and $n = 1$, respectively), should be contributed by the unbound orbit of the energy larger than $V_{\max}$ and the boundary orbit of energy equal to $V_{\max}$, respectively. The latter orbit is the so-called separatrix orbit or the stable-unstable manifolds W^s-W^u, which is shown by the red bold curve coming from the infinity to pass through S and finally returning to the infinity after passing through S again. Indeed, one can recognize that the Husimi plot of the eigenfunction with $n = 12$ has the major distribution flowing outside of W^s-W^u, whereas the Husimi plots for the eigenfunctions $n = 9$ and $n = 1$ indicate that the major part flows along the W^s-W^u complex. All the above observations by the Husimi plot for the Hénon map are consistent with the successive transition scenario due to the multiquanta excitation processes confirmed for the standard map. A more quantitative verification for the claim, similar to Fig. 6(c), will be demonstrated in Appendix B.

IV. CONCLUDING REMARKS

Applying the BHC expansion, nonintegrable quantum maps are transformed into one-dimensional integrable Hamiltonians (BHC Hamiltonian) with great accuracy in the nearly integrable regime. Based upon the integrable Hamiltonian, the lowest-order quantum perturbation theory using the residual interaction as the perturbation can reproduce details of the transition from the instanton (I) tunneling to a noninstanton (NI) tunneling, and the characteristics of the tunneling probability beyond the transition region. In particular, the lowest order perturbation calculation clarifies the underlying structure of the tunneling characteristics. The structure forms a staircase, each step of which is composed of two regions called the plateau and the steep-slope regions.

The dominant part of the time-evolution operator of quantum map is renormalized as the one-dimensional integrable BHC Hamiltonian, and the residual interaction of the evolution operator, which is represented as the transition matrix element (TME), decreases in general with the order of the approximation. However, certain particular components of the TME become invariant against the renormalization. The energies of the modes forming the invariant components are energetically separated by integer multiples of the fundamental quanta $\Omega\hbar$ of the quantum map, and broad peaks are formed around the invariant components, which implies that the resonant interaction with the fundamental period of the quantum map remains invariant, never being renormalized as the integrable part.

Further, an important fact is that the amplitudes of the invariant components are quasiclassical in the sense that they are insensitive to the Planck constant and exhibit an essentially singular dependence upon the nonintegrability parameter, which is similar to the Melnikov integral measuring the dimension of real classical chaos formed close to the separatrix.

The resonance peak components of the transition matrix selectively connect the mode $|u_n^{(M)}\rangle$ with the modes in the broad peak, forming a new tunneling channel. The tunneling amplitude of the channel is almost equal to the the height of the TME resonance peak and is quasiclassical and further has a Melnikov-integral-like singular dependency upon the perturbation parameter. The new tunneling channel wins the competition with the instanton channel as the quantum number decreases from the top; it is the instanton-noninstanton (I-NI) transition.

Selective excitation of the modes occurs also at a higher-harmonic resonance, and a new tunneling channel is formed there, and the successive switching among the harmonic channels with decrease in the quantum number is the origin of the staircase structure characteristic in the tunneling probability. Such a mechanism can be called the resonant multiquanta excitation mechanism. If the selected mode has energy larger than $V_{\max}$, the tunneling probability is almost independent of the quantum number n, forming the plateau region, while if the selected channel has energy less than $V_{\max}$, the tunneling probability decreases with n steeply like the instanton. A pair of a plateau region and a steep-slope region together form each step of the staircase structure as mentioned above.

In a closed system like the standard map, the role of the resonant multiquanta excitation mechanism is very clearly seen in Fig. 6. However, in open systems such as the Hénon map, the existence of the multiquanta excitation mechanism is not recognizable explicitly, but a careful analysis reveals that the same mechanism works also in the Hénon map, as is shown in Appendix B.

The invariant component of the TME exhibits a Melnikov integral-like singular dependency upon the nonintegrability parameter. This fact implies that the unrenormalized interaction describes the intrinsically nonintegrable dynamics of the nearly integrable quantum map. On the other hand, these components work so as to induce the new tunneling mechanism via the resonant multiquanta excitation, which replaces the instanton tunneling mechanism. These observations support our conjecture that the classical nonintegrability first manifests itself as the tunneling phenomenon.

In the nearly integrable regime, the eigenfunction of the BHC Hamiltonian approximates the exact eigenfunctions of quantum map very well in the classically accessible region. In contrast to this, the tunneling component of the eigenfunction is very sensitive to the change of parameters, and the integrable model of the tunneling, i.e., the instanton, does no longer work well. This fact implies that although the classical invariant manifold supporting the quantized wave function has

a sound analyticity in the real domain, as is expected by the KAM theory, its extension into the complex domain is ill-structured and loses analyticity completely. This structure in classical dynamics and its manifestation in quantum dynamics is a fundamental problem that should be clarified. This is the very reason why we study tunneling.

ACKNOWLEDGMENTS

We are grateful for useful discussions with K. Takahashi and N. Mertig. This work is partly supported by the Japanese people's tax via JPSJ KAKENHI Grants No. JP15H03701 and No. JP16K17767, and the authors would like to acknowledge the Japanese people. We also would like to thank KANKIKAI for permission to use particular facilities during this study.

APPENDIX A: EVALUATION OF r

We have to note here that in the limit of $\delta E \to 0$ the period $T(\delta E) = 2\pi/\omega(\delta E)$ diverges logarithmically as shown by Eq. (39). From Eq. (40), the relation between δE and δI is given by

$$\delta I/A_0 = \delta E f(\delta E), \tag{A1}$$

by introducing the function $f(\delta E)$ defined by

$$f(\delta E) = -\ln \delta E + A_1/A_0 + 1 + O(\delta E).$$

Then differentiating both sides of Eq. (A1) by δE, we obtain the orbital frequency

$$\omega(\delta E) = \frac{1}{A_0[f(\delta E) - 1 + O(\delta E)]}. \tag{A2}$$

With the above equation and the edge state condition $\delta E_n = \hbar\Omega$, the energy $\delta E'$ corresponding to $\delta I_n/2$ is decided by

$$\delta E' f(\delta E') = \frac{\delta I_n}{2A_0} = \frac{\Omega\hbar}{2} f(\Omega\hbar). \tag{A3}$$

The effective frequency of the Fourier integral Eq. (27) is given by $\Omega_{\rm eff} = \delta n\omega(\delta I_n/2) = \omega(\delta E')\delta I_n/\hbar$, and its ratio to the frequency Ω is expressed by

$$r := \frac{\Omega_{\rm eff}}{\Omega} = \frac{f(\Omega\hbar)}{f(\delta E') - 1 + O(\delta E)}. \tag{A4}$$

Here the expression (A2) for $\delta E'$ and Eq.(A1), for which δE and δI are replaced by $\Omega\hbar$ and δI_n, respectively, are used. In the semiclassical limit $\hbar \ll 1$, $|f(\delta E')| \gg 1$ due to the logarithmic divergence, and Eq. (A4) is approximated by using Eq. (A1):

$$r \sim \frac{f(\Omega\hbar)}{f(\delta E')} = \frac{2\delta E'}{\Omega\hbar}. \tag{A5}$$

Now we have only to evaluate $\delta E'$ in terms of $\Omega\hbar$, which can be achieved by solving Eq. (A3). Its root can be obtained by the iteration procedure $x \to x'$:

$$x' = \frac{\frac{\Omega\hbar}{2} f(\Omega\hbar)}{f(x)}, \tag{A6}$$

with a proper initial input. If we start with $x = \Omega\hbar$, the approximate root is

$$\delta E' \sim \frac{\frac{\Omega\hbar}{2} f(\Omega\hbar)}{f\frac{\Omega\hbar}{2}\left[\frac{f(\Omega\hbar)}{f(\Omega\hbar/2)}\right]}. \tag{A7}$$

Substitution of this into Eq. (A5) yields

$$r \sim \frac{1}{1 + \frac{1}{f(\Omega\hbar)} \ln \frac{2f(\Omega\hbar/2)}{f(\Omega\hbar)}} \ (< 1). \tag{A8}$$

In the limit of $\hbar\Omega \ll 1$, $f(x) \sim -\ln(x)$ and

$$r \sim \frac{1}{1 + \frac{1}{|\ln(\Omega\hbar)|} \ln |2\ln(\Omega\hbar/2)/\ln \Omega\hbar|}. \tag{A9}$$

APPENDIX B: A FEW MODES ANALYSIS: THE HÉNON MAP

In the following analysis we take the best approximate wave function $\psi_n^{(M),k_{\rm max},{\rm few}}(q)$ defined by Eqs. (54) and (55) composed of a few number modes, based upon the few mode hypothesis of Sec. III F. In Fig. 7 we compared the tunneling amplitude of the approximate wave function $\psi_n^{(M),k_{\rm max},{\rm few}}(q)$ with that of the eigenfunction obtained by the perturbation theory for which all modes are taken into account. The agreement is good, and the few mode hypothesis is acceptable.

Recall the error ${\rm Err}(j_1^*, j_2^*, \ldots, j_{k_{\rm max}}^*)$ $(j_1^* < j_2^* \cdots < j_{k_{\rm max}}^*)$ defined by Eqs. (54) and (55) as the distance of $\psi_n^{(M),k_{\rm max},{\rm few}}(q)$ from the exact eigenfunction in the tunneling region $\mathcal{T}$. Here we remove a certain mode j_k^* from the optimal set and construct the approximate wave function by them and measure the defective distance ${\rm Err}(j_1^*, \ldots, j_{k-1}^*, j_{k+1}^*, \ldots, j_{k_{max}}^*)$. Then we define the relative difference as

$$z_{j_k^*} = |{\rm Err}(j_1^*, \ldots, j_{k-1}^*, j_{k+1}^*, \ldots, j_{k_{\rm max}}^*)/ {\rm Err}(j_1^*, j_2^*, \ldots, j_{k_{\rm max}}^*) - 1|, \tag{B1}$$

which is normalized by the minimal error. It measures the relative weight of the contribution from j_k to the optimal construction of $\psi_n^{(M),k_{\rm max},{\rm few}}(q)$. We call the set $\{z_{j_1^*}, z_{j_2^*}, \ldots, z_{j_{k_{\rm max}-1}^*}, z_{j_{k_{\rm max}}^*}\}$ the defect spectrum.

We show in Fig. 9 the defect spectrum, making correspondence with the contribution spectrum of the standard map shown in Fig. 6. The variation of the spectrum with the quantum number n shows a surprisingly similar behavior to that of the contribution spectrum of the standard map in Fig. 6. If n is not far from $n_{\rm max}$, the peak is at the mode n itself, which means the instanton tunneling tail of $u_n^{(M)}(q)$ dominates the tunneling. However, as n is reduced, the dominant part of the spectrum shifts to the location of the first resonance $E_1^{\rm Res}(E_n) = E_n + \Omega\hbar$ which is larger than $V_{\rm max}$. This is the I-NI transition. With further decrease of n the dominant part of the defect spectrum moves along the first resonance line.

If $E_1^{\rm Res}(E_n) > V_{\rm max}$, the principal modes are unbound and the tunneling amplitude is in the plateau regime, whereas if $E_1^{\rm Res}(E_n) < V_{\rm max}$ the principal modes are bound and the tunneling amplitude is in the steep-slope region.

As n decreases further, the dominant part of the defect spectrum shifts from the first resonance line to the second

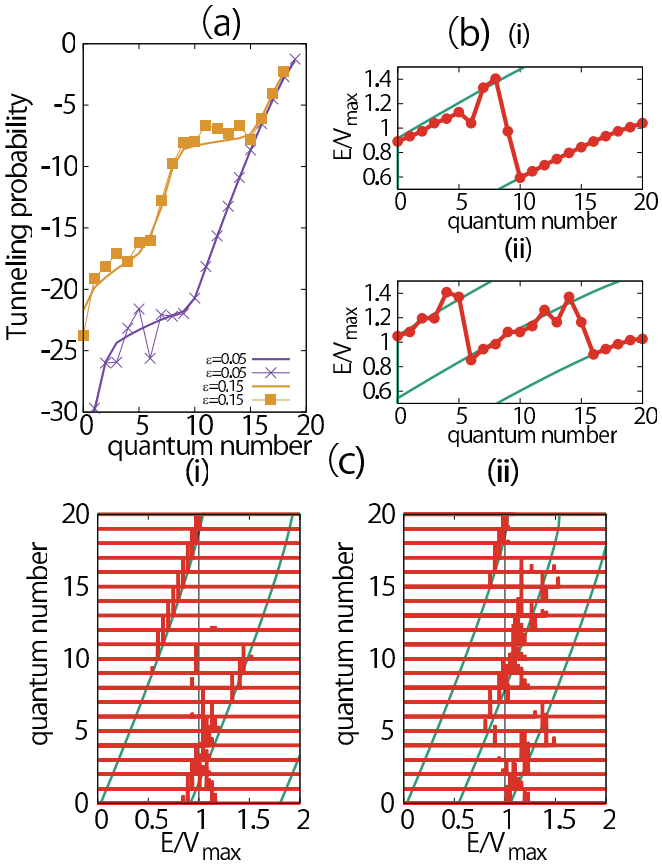

FIG. 9. (a) The tunneling probability computed only by the most influential mode of the defect spectrum almost reproduces the precise results for $\epsilon = 1.5$ and 0.050. (b) The energy eigenvalue of the most influential mode as a function of quantum number n (line with points) are compared with the harmonic resonance lines $E_\ell^{\mathrm{Res}}(n)$ (solid lines) for $\ell = 0, 1, 2$, and 3. (c) The defect spectrums for all the quasibound states of quantum number $0 \leqslant n \leqslant n_{\max}$. The spectrum is expressed as a function of normalized energy, and the solid lines indicate the location of the ℓth resonance, i.e., $E_\ell^{\mathrm{Res}}(n)$ for $\ell = 0, 1, 2$, and 3.

resonance one, i.e., $E_2^{\mathrm{Res}}(E_n) = E_n + 2\Omega\hbar$, and then with decrease of n, a transition similar to the one observed at the I-NI transition occurs, and a plateau structure followed by a steep-slope region emerges again in the tunneling characteristic. Figure 9(b) depicts the energy of the most influential mode in the defect spectrum as the function of n, which summarizes the successive switching of the energy of the most dominant mode among the resonance lines discussed above.

In Fig. 9(a) we compare the tunneling probability computed only by the most dominant mode of the defect spectrum with the exact result. As is the case of the standard map, the single-mode approximation almost reproduces the feature of tunneling characteristics. However, one can see that in the plateau region the single-mode approximation significantly exceeds the exact results, which means that the single-mode approximation is insufficient, and cancellation among several dominant modes is essential in the case of the Hénon map.

This is a notably different feature from the standard map. As has been repeatedly stressed, the dominant mode is selected first by the broad peak of TME. It is reinforced by the quantum resonance factor R_{nj}, which is broader in the case of the Hénon map because the modes $E_1^{\mathrm{Res}}(E_n) > V_{\max}$ escape toward $q = -\infty$. This is the reason why the most dominant mode approximation is bad particularly in the plateau region of the Hénon map. The standard map has no escaping region.

Consequently, even in the case of the Hénon map, in which the contribution spectrum analysis cannot extract the principal modes, the defect spectrum analysis successfully reveals that the tunneling characteristics is explained by the multiquanta excitation and competitions among them.

APPENDIX C: FULLY CLASSICAL CONSTRUCTION OF THE TRANSITION MATRIX ELEMENT

Let $\hat{H}(\hat{X}, t)$ be the original time-dependent Hamiltonian of period $\tau = 2\pi/\Omega = \sqrt{\epsilon}$ generating the time-evolution operator $\hat{U} = \mathcal{T}\exp\{-\int_0^\tau i\hat{H}(t')\,dt'/\hbar\}$, where $\hat{X}$ represents the quantal version of classical canonical variables such as (q, p) or the action-angle variables (I, θ). We introduce an integrable Hamiltonian $\hat{H}_0(p, q)$ which approximates well the dynamics of the explicitly time-dependent Hamiltonian $\hat{H}(\hat{X}, t)$ and defines the residual part of the Hamiltonian:

$$\Delta\hat{H}(\hat{X}, t) = \hat{H}(\hat{X}, t) - \hat{H}_0(\hat{X}). \tag{C1}$$

Then the perturbation expansion in the interaction picture yields

$$\hat{U} = e^{-iH_0/\hbar}\Big[1 - i/\hbar\int_0^\tau dt\,\Delta\hat{H}_{\mathrm{i}}(t) + (i/\hbar)^2\int_0^\tau dt_1\int_0^{t_1} dt_2\,\Delta\hat{H}_{\mathrm{i}}(t_1)\Delta\hat{H}_{\mathrm{i}}(t_2) + \cdots\Big], \tag{C2}$$

where $\Delta\hat{H}_{\mathrm{i}} = e^{i\hat{H}_0 t/\hbar}\Delta H(t)(\hat{X}, t)e^{-i\hat{H}_0 t/\hbar}$ is the interaction representation.

We consider only the lowest order terms, because the BHC expansion is very nice for $M \gg 1$, and derive the fully classical formula for the TME. Let us consider

$$\langle u_j|\Delta\hat{H}_{\mathrm{i}}(t)|u_n\rangle = e^{iE_j t/\hbar}\langle u_j|\Delta H(t)(\hat{X}, t)|u_n\rangle e^{-iE_n t/\hbar}.$$

Applying the correspondence principle Eq. (27), it is represented by

$$\langle u_j|\Delta\hat{H}_{\mathrm{i}}(t)|u_n\rangle = \frac{1}{T}e^{i(E_j - E_n)t/\hbar} \times \int_0^T \Delta H[X(I, t'), t]e^{i(n-j)\omega t'}\,dt',$$

where I, ω, and T are shorthand notation for action $I_{nj} = (I_n + I_j)/2$, frequency $\omega \equiv \omega_{nj} = dH_0(I)/dI|_{I=I_{nj}}$, and the period $T \equiv T_{nj} = 2\pi/\omega_{nj}$ of the classical orbit $X(I, \omega t') = X(I_{nj}, \omega_{nj}t)$ described by the classical integrable Hamiltonian $\hat{H}_0$, and $\Delta H(X, t)$ is the classical counterpart of $\Delta\hat{H}(\hat{X}, t)$. The above expression is approximated by using Eq. (29), i.e., $(E_j - E_n) \simeq (j - n)\omega_{jn}$ as

$$\langle u_j|\Delta\hat{H}_{\mathrm{i}}(t)|u_n\rangle = \frac{1}{T}\int_0^T \Delta H[X(I, t' + t), t]e^{i(n-j)\omega t'}\,dt'.$$

Thus the TME can in principle be computed by using the classical orbit

$$\langle u_j|\hat{U}|u_n\rangle = -e^{-iE_j t/\hbar}\frac{i}{T\hbar}\int_0^\tau\int_0^T \Delta H \times [X(I,t'+t),t]e^{i(n-j)\omega t'}\,dt'\,dt. \quad \text{(C3)}$$

Such a classical representation can be extended to higher-order terms.

APPENDIX D: RELATIONSHIP AND DIFFERENCE BETWEEN RAT APPROACH AND OURS

Here we discuss the relation between our approach and the RAT approach [25–32], and the difference in the physical interpretations. In the nearly integrable regime, the separatrix still remains, so there is an exponentially narrow chaotic region. As was emphasized in Secs. III C and III E and in previous publications [33,34] the tunneling in the plateau region is dominated by the transition between inside and outside of the separatrix, and so the RAT theory, which is based on the action-angle representation inside the separatrix, cannot in principle be applied.

The region in which the RAT approach and ours can be compared is the first steep-slope region. Confining ourselves to this region, we relate our approach to the RAT approach. In particular we here try to interpret the observed TME in the BHC representation from the viewpoint of a hypothesis that underlies the RAT theory. The classical nonlinear resonance terms are contained in the Fourier expansion of the classical counterpart $\Delta H := H(X,t) - H_0(X)$ defined by Eq. (C1). Recalling that $H(X,t+\tau) = H(X,t)$, the Fourier expansion is written as

$$\Delta H(X[I,\theta/\omega(I)],t) = \sum_{\ell,m\in\text{integer}^2}\{V_{\ell,m}(I)e^{i(\ell\theta+m\Omega)t} + \text{c.c.}\}, \quad \text{(D1)}$$

where $\Omega = 2\pi/\tau$. The Fourier coefficient $V_{\ell,m}$ can in principle be computed by the time-dependent data $\Delta H[X(I,t),t']$ for every orbit $X(I,t)$ specified by the action I and the frequency $\omega(I)$. Substituting Eq. (D1) into the formula (C3), we immediately obtain the classical expression of the TME in terms of the Fourier coefficient $V_{\ell,m}$:

$$\langle u_j|\hat{U}|u_n\rangle = -e^{-iE_j t/\hbar}\sum_m \frac{1}{\hbar}V_{j-n,m}(I_{nj})\frac{e^{i(\omega_{nj}(j-n)+m\Omega)\tau}-1}{\omega_{nj}(j-n)+m\Omega}. \quad \text{(D2)}$$

The factor in the r.h.s. may be replaced by

$$\frac{e^{i(\omega_{nj}(j-n)+m\Omega)\tau}-1}{\omega_{nj}(j-n)+m\Omega} \simeq \frac{e^{i((E_j-E_n)/\hbar+m\Omega)\tau}-1}{(E_j-E_n)/\hbar+m\Omega}. \quad \text{(D3)}$$

The resonance enhancement occurs at $(j-n)\omega = -m\Omega$. In the RAT treatment, the nonlinear resonances which are "visible" in the sense that the sizes are much larger than the Planck cell in a classical phase space are chosen, and the local Hamiltonian is constructed around each resonance satisfying $\omega r = \Omega s$ by applying the secular perturbation technique [25]. The corresponding amplitude $V_{j-n=r,m=-s}$ is determined numerically so as to reproduce the classical resonance pattern in phase space.

For simplicity, we suppose $s = 1$ and take only a single resonance with a given r, then the classical resonance condition $r\omega(I_{n,n+r}) \sim \Omega$ is satisfied [25]. From Eq. (D3) this situation also corresponds to our resonance condition $E_1(E_n) = E_j$. In such a case the RAT approach considers only a single resonance term with $V_{r,-1}$, meaning that we ignore all the contributions except for the mode $j = n + r$ in the perturbation formula Eq. (20).

Such a reduction is, however, unreasonable in our situation because of the following reasons. In the semiclassical limit, the relevant eigenstate's energy E_n at which the I-NI transition occurs is close to $V_{\max}$, and the corresponding classical frequency $\omega(I_n)$ approaches 0, and $r \sim \Omega/\omega(I_n)$ may be much larger than 1 in general. Indeed, Fig. 4 suggests that $r > 10$, which means that the mode with $j - n = r \pm 1, r \pm 2, \ldots$ can also be nearly resonant with Ω. In other words, once a resonance term with a large r exists, we have to take into account the nearby resonances such as $r \pm 1 : 1\, r \pm 2 : 1, \ldots$ with the amplitude $V_{r,-1}$ which is slowly varying with r. They contribute to TME with the weights comparable to that of r, which are proportional to the factor (D3) and form the broad resonance peak. In the above mentioned case there is no predominant resonance, and it is a typical situation in the nearly integrable regime treated in the present paper. But if the perturbation strength is not weak enough, a particular classical resonance is more prominent than others and is classically "visible", which is the ideal case for the RAT approach. Even in such a case, we found that the TME exhibits a broad peak and does not have a corresponding prominent peak [37].

The existence of the broad peak of TME, which was the essential result of the BHC renormalization, means that all the $|j-n|:1$ classical resonances corresponding to the quantum number j in the broad peak contribute as the noninstanton tunneling channels. The above argument holds also for the higher-order steps of the tunneling staircase: in the second step region, the $|j-n|:2$ resonances contributes, and the $|j-n|:3$ resonances in the third step and so on, contributing as a multiquanta excitation process. Such direct processes are ignored in the RAT approach [28]. If we consider the higher-order corrections of Eq. (C2) neglected here, the combination of $|j-n|:1$ resonances, which is taken into account in the RAT approach [25], also contributes to higher-harmonic resonances. But in this case, contributions come from not a particular combination of modes but many possible combinations of the modes in the broad peak.

As stressed in the arguments of Sec. III E and Appendix B, particularly around Figs. 6 and 9, the maximally contributing mode seems to lead the multiquanta excitation mechanism in a qualitative sense. Quantitatively, however, a number of modes in the broad peak participate in the tunneling to form a characteristic wave function in the tunneling region. In the above respects our result takes in all the mainly contributing

modes in the broad peak, almost of which are neglected in the RAT theory because of a classical mechanical reason. The relation of our approach to the RAT approach will be discussed in more detail in a forthcoming paper.

[1] H. Poincaré, *Les Méthodes nouvelles mécanique céleste, 3 vols.* (Gauthier-Villars, Paris, 1888–1892); *New Methods of Celestical Mechanics* (American Institute of Physics, Melville, 1992).

[2] See, for example, V. I. Arnol'd, Russ. Math. Surv. **18**, 9 (1963).

[3] J. Guckenheimer and P. Holmes, *Nonlinear Oscillations, Dynamical Systems, and Bifurcation of Vector Fields* (Springer-Verlag, New York, 1983).

[4] B. V. Chirikov, Phys. Rep. **52**, 263 (1979).

[5] L. S. Schulman, *Techniques and Applications of Path Integration* (Wiley Interscience, New York, 1996).

[6] M. C. Gutzwiller, *Chaos in Classical and Quantum Mechanics* (Springer-Verlag, New York, 1990).

[7] S. Morosawa, Y. Hishimura, M. Taniguchi, and T. Ueda, *Holomorphic Dynamics* (Cambridge University Press, Cambridge, 1999).

[8] J. M. Greene and I. C. Percival, Physica D **3**, 530 (1981); I. C. Percival, *ibid.* **6**, 67 (1982).

[9] S. C. Creagh, in *Tunneling in Two Dimensions* in *Tunneling in Complex Systems*, edited by S. Tomsovic (World Scientific, Singapore, 1998), p. 35.

[10] M. Wilkinson, Physica D **21**, 341 (1986).

[11] S. C. Creagh, J. Phys. A **27**, 4969 (1994).

[12] A. Shudo and K. S. Ikeda, Phys. Rev. Lett. **109**, 154102 (2012).

[13] S. Tomsovic, *Tunneling in Complex Systems* (World Scientific, Singapore, 1998).

[14] S. Keshavamurthy and P. Schlagheck, *Dynamical Tunneling: Theory and Experiment* (CRC Press, Boca Raton, FL, 2011).

[15] A. Shudo and K. S. Ikeda, Phys. Rev. Lett. **74**, 682 (1995); Prog. Theor. Phys. Suppl. **116**, 283 (1994); Physica D **115**, 234 (1998).

[16] S. Adachi, Ann. Phys. **195**, 45 (1989).

[17] A. Shudo, Y. Ishii, and K. S. Ikeda, J. Phys. A **35**, L225 (2002); **42**, 265101 (2009); **42**, 265102 (2009).

[18] A. Shudo, Y. Ishii, and K. S. Ikeda, Europhys. Lett. **81**, 50003 (2008).

[19] W. A. Lin and L. E. Ballentine, Phys. Rev. Lett. **65**, 2927 (1990).

[20] O. Bohigas, S. Tomsovic, and D. Ullmo, Phys. Rep. **223**, 43 (1993).

[21] S. Tomsovic and D. Ullmo, Phys. Rev. E **50**, 145 (1994).

[22] K. Takahashi and K. S. Ikeda, Ann. Phys. **283**, 94 (2000).

[23] K. Takahashi and K. S. Ikeda, Europhys. Lett. **71**, 193 (2005); J. Phys. A **41**, 095101 (2008).

[24] K. Takahashi and K. S. Ikeda, Phys. Rev. A **79**, 052114 (2009).

[25] O. Brodier, P. Schlagheck, and D. Ullmo, Phys. Rev. Lett. **87**, 064101 (2001); Ann. Phys. **300**, 88 (2002).

[26] C. Eltschka and P. Schlagheck, Phys. Rev. Lett. **94**, 014101 (2005).

[27] A. Mouchet, C. Eltschka, and P. Schlagheck, Phys. Rev. E **74**, 026211 (2006).

[28] P. Schlagheck, A. Mouchet, and D. Ullmo, in *Dynamical Tunneling: Theory and Experimental*, edited by S. Keshavamurthy and P. Schlagheck (CRC Press, Boca Raton, FL, 2011), Vol. 8, p. 177.

[29] S. Löck, A. Bäcker, R. Ketzmerick, and P. Schlagheck, Phys. Rev. Lett. **104**, 114101 (2010).

[30] A. Bäcker, R. Ketzmerick, and S. Löck, Phys. Rev. E **82**, 056208 (2010).

[31] J. L. Deunff, A. Mouchet, and P. Schlagheck, Phys. Rev. E **88**, 042927 (2013).

[32] N. Mertig, J. Kullig, C. Löbner, A. Bäcker, and R. Ketzmerick, Phys. Rev. E **94**, 062220 (2016).

[33] Y. Hanada, A. Shudo, and K. S. Ikeda, Phys. Rev. E **91**, 042913 (2015).

[34] A. Shudo, Y. Hanada, T. Okushima, and K. S. Ikeda, Europhys. Lett. **108**, 50004 (2014).

[35] The optimal M depends on $|s|$. Roughly, it is more or less 9–11 for the standard map and more than 21 for the Hénon map.

[36] J. J. Morehead, Phys. Rev. A **53**, 1285 (1996).

[37] Comparing the expression Eq. (D2) with our numerically computed TME, we can evaluate the coefficient of the Fourier expansion $|V_{j-n,-1}|$. It does not decay exponentially with $|j-n|$ but keeps almost the same magnitude for the modes j with energy less than the first resonance, i.e., $E_n < E_j < E_n + \Omega\hbar$, if the BHC basis of large M is used for the TME. In other words, the broad peak is decided by the factor (D3).